Compliant Control of Multicontact and Center-of-Mass Behaviors in Humanoid Robots

Luis Sentis, *Member, IEEE*, Jaeheung Park, *Member, IEEE*, and Oussama Khatib, *Fellow, IEEE*

***Abstract*—This paper presents a new methodology for the analysis and control of internal forces and center-of-mass (CoM) behavior, which are produced during multicontact interactions between humanoid robots and the environment. The approach leverages the virtual-linkage model that provides a physical representation of the internal and CoM resultant forces with respect to reaction forces on the supporting surfaces. A grasp/contact matrix describing the complex interactions between contact forces and CoM behavior is developed. Based on this model, a new torque-based approach for the control of internal forces is suggested and illustrated on the Asimo humanoid robot. The new controller is integrated into the framework for whole-body-prioritized multitasking, thus enabling the unified control of CoM maneuvers, operational tasks, and internal-force behavior. The grasp/contact matrix is also proposed to analyze and plan internal force and CoM control policies that comply with frictional properties of the links in contact.**

***Index Terms*—Humanoid robots, multicontact behaviors, prioritized control.**

I. Introduction

AN IMPORTANT problem in humanoids is their ability to manipulate and maneuver in their environments through whole-body multicontact interactions. This ability is a necessary skill that enables humanoids to operate dexterously in human environments using their whole bodies. For example, see the interaction shown in Fig. 1. To address this challenge, we analyze here the complex interdependencies between whole-body contacts and their relationship with center-of-mass (CoM) and task behaviors. We create contact models using the virtual-linkage model [35], which describes the relationship between resultant and reaction forces, pressure points, and internal tensions between closed loops. We analyze the dynamics of internal forces and use the virtual-linkage model to create a controller that regulates them to desired values. We integrate the proposed control methods with our framework for prioritized multitasking [29], addressing the unified control of constraints, CoM maneuvers, operational tasks, postures, and internal forces.

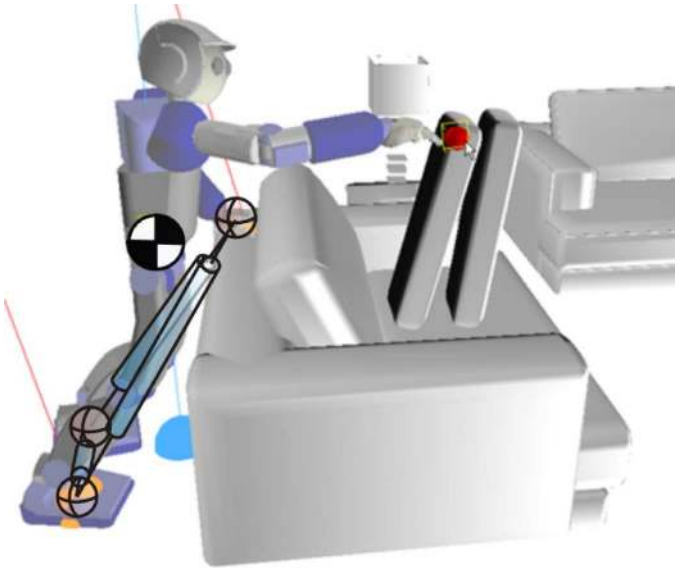

Fig. 1. Real-time simulation of a multicontact behavior with user-enabled interactive control of the robot's right hand. A virtual-linkage model is overlaid, capturing the internal-force behaviors acting between supporting bodies. The black and white circle corresponds to the robot's CoM position, which is placed above the stability area determined by the three supporting contacts.

The contributions of this work are as follows: 1) An in-depth analysis and modeling of CoM and internal-force behavior with respect to surface-friction properties; 2) identification of the torque manifold associated with contact closed loops and the development of feedback controllers to regulate internal-force behavior; and 3) the analysis of the conditions of friction stability as well as contact rotational behavior with respect to CoM and internal-force behaviors.

Since the early 1980s, contact interactions in robots have been addressed, with work on dynamics and force control in the context of robotic manipulation [15] [25]. Cooperative distributed manipulation became important to enable the handling of heavy objects [1]. To describe the behavior of the object independently of the manipulators, an augmented object model was proposed based on dynamically consistent representations [17]. Research began to focus on modeling multigrasp behaviors and the associated internal forces acting between manipulators [21]. Using a closed-chain mechanism, which is called the virtual-linkage model, decoupled-object behavior and accurate dynamic control of internal forces were addressed [35]. Mobile robotic platforms equipped with robotic manipulators were developed [12], and multigrasp manipulation was implemented using efficient

Manuscript received October 7, 2008; revised March 31, 2009, November 29, 2009, and February 14, 2010; accepted February 4, 2010. Date of publication April 19, 2010; date of current version June 9, 2010. This paper was recommended for publication by Associate Editor K. Yamane and Editor J. Paul upon evaluation of the reviewers' comments. This work was supported by the Honda Motor Company.

L. Sentis is with the Department of Mechanical Engineering, The University of Texas at Austin, Austin, TX 78712 USA (e-mail: luis.sentis@austin.utexas.edu).

J. Park is with the Department of Intelligent Convergence Systems, Seoul National University, Seoul 443-270, Korea (e-mail: park73@snu.ac.kr).

O. Khatib is with the Department of Computer Science, Stanford University, Stanford, CA 94305 USA (e-mail: ok@cs.stanford.edu).

Color versions of one or more of the figures in this paper are available online at http://ieeexplore.ieee.org.

Digital Object Identifier 10.1109/TRO.2010.2043757

operational-space algorithms [4]. The dynamics and control of task and postural behaviors in humanoid robots were addressed and prioritized multitask controllers were developed to enable the unified force-level control of constraints, task, and postures [28].

The aim of this new research is to analyze and model whole-body multicontact interactions and provide a control platform that enables humanoids to manipulate and maneuver efficiently in their environments. It is, therefore, important to understand the relationship between reaction forces on contact bodies, internal tensions and moments acting between these contacts, and whole-body task and motion behaviors. Because this work connects with legged locomotion, it is useful to review modern developments in this area. Since the 1960s, dynamic legged locomotion has been a center of attention [8]. The zero-moment point criterion (ZMP) was developed to evaluate CoM acceleration boundaries [33]. Implementations of simple dynamic-control algorithms for multilegged running robots followed the method given in [24]. ZMP methods for humanoid robots were pioneered around the same times [30], [31] and later perfected as part of the Honda humanoid program [11]. To enable generalized multicontact-locomotion behaviors, extensions to the ZMP dynamic-evaluation criterion were developed [10]. Compliant multicontact behaviors using optimal distribution of contact forces has recently been explored [13]. For multilegged systems, finding CoM-static placements given frictional constraints was tackled in [2] and [5]. The field of legged locomotion is vast and continues to broaden with pioneering contributions in areas such as hybrid nonlinear control [32], [34], biomimetic-coupled oscillators [3], [14], and passive dynamic walking [6], [20].

In this paper, we analyze and control the interactions between whole-body contacts, CoM, and task behaviors. We define multiple centers of pressure (CoP's) to abstract the behavior of contact bodies. When the CoP of a contact body approaches an edge, a nonzero moment takes place about that edge causing the body to rotate. By controlling the position of contact CoP's, we control contact rotational behavior. We use the virtual-linkage model to describe multicontact and CoM whole-body behaviors. We define a grasp/contact matrix to establish the relationship between resultant forces at the CoM and internal and reaction forces on contact bodies. We create dynamically correct controllers to govern the behavior of contact CoP's, internal tensions, and normal moments. Using control structures that are orthogonal to CoM and task behavior, we integrate internal-force controllers with our previous framework for prioritized multitask control.

The capabilities and effectiveness of our methods are validated through whole-body multicontact simulations performed on a dynamical simulator of the Honda Asimo robot. CoM tracking, fulfillment of contact constraints, and internal-force control are achieved with high accuracy.

II. Modeling of Internal Forces and Centers of Pressure and Center-of-Mass Behavior Using the Virtual-Linkage Model

The objective of this section is to analyze multicontact interactions between a humanoid robot and its environment and to develop contact models that fully characterize the contact state of the robot. We first assign multiple contact CoP's associated with each contact extremity. Because contact CoP's are points with zero tangential moments, we use them to evaluate and control contact rotational stability. Ensuring that all contact CoP's stay within contact boundaries prevents unwanted edge rotations of the links in contact. We develop contact models using the virtual-linkage model defined with respect to CoP positions and relate CoM and internal-force behavior with respect to contact forces. These models are then used in the next section to control the robot's overall contact state and CoM behavior.

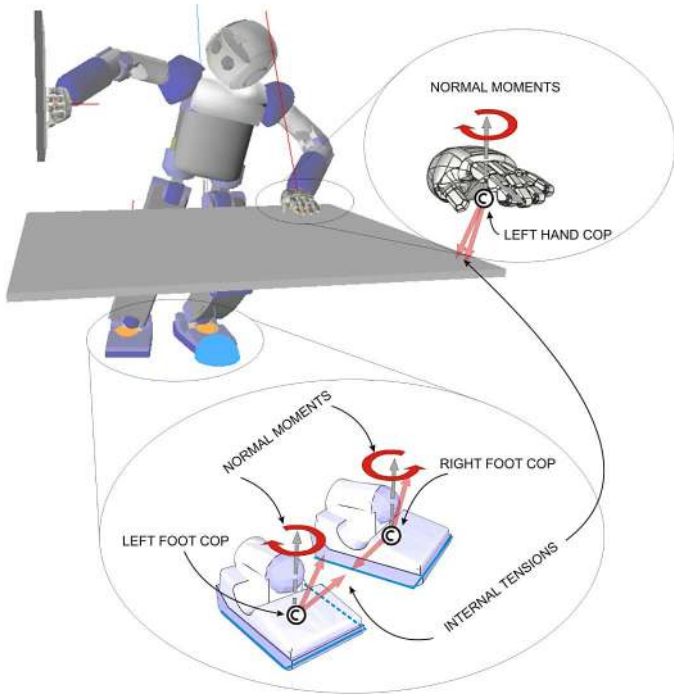

Fig. 2. Decomposition of internal forces and moments. We decompose internal forces and moments into contact CoP's, internal tensions, and normal moments. Contact CoP's allow us to control contact rotational behavior, while internal tensions and normal moments allow us to control the behavior of contact points with respect to surface-friction properties.

We consider whole-body contact scenarios where multiple extremities of the robot are in stable contact against flat surfaces (see Fig. 2). In this case, every contact imposes six constraints on the robot's mobility. We assume that each extremity in contact has enough joints with respect to the base link to enable the independent control of its position and orientation. This condition translates into the existence of six or more independent mechanical joints between the base link and the extremity in contact. We consider contact scenarios involving an arbitrary number of supporting extremities, which is represented by the number n_s. Flat supporting contacts impose $6n_s$ constraints on the robot's motion, where six of these constraints provide the support to maneuver the robot's CoM and the other $6(n_s - 1)$ describe the internal forces and moments acting on the closed loops that exist between supporting extremities [35]. Internal forces and moments play two different roles in characterizing the contact behavior of the robot: 1) Contact CoP's define the behavior of the contact links with respect to edge or point rotations, and

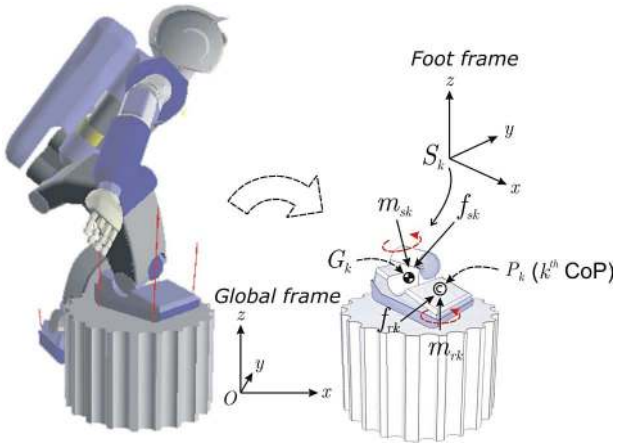

Fig. 3. Forces acting on a supporting body (e.g., the right foot). Establishing the balance of moments on each contact body allows us to determine the position of contact CoP's.

2) internal tensions and moments describe the behavior of the contact links with respect to the friction characteristics associated with the contact surfaces.

A. Center of Pressure Points

For a number of n_s links in contact, we associate n_s contact CoP's. Each contact CoP is defined as the 2-D point on the contact surface where tangential moments are equal to zero. Therefore, $2n_s$ coordinates describe all contact pressure points. In Fig. 2, we illustrate a multicontact scenario involving three supporting contacts on the robot's feet and left hand, and an operational task designed to interact with the robot's right hand. We focus on the analysis of the forces and moments taking place on a particular contact body (see Fig. 3). Based on the studies of Vukobratović and Borovac [33], we abstract the influence of the robot's body above the kth supporting extremity by the inertial and gravity force f_{s_k}, and the inertial and gravity moment m_{s_k} acting on a sensor point S_k. For simplicity, we assume that the sensor is located at the mechanical joint of the contact extremity. Here, P_k represents the contact CoP of the kth contact extremity, f_{r_k} is the vector of reaction forces acting on P_k, and m_{r_k} is the vector of reaction moments acting on P_k. The frame $\{O\}$ represents an inertial frame of reference located outside of the robot and the frame $\{S_k\}$ represents a frame of reference located at the sensor point. All force quantities are described with respect to the sensor frame. Assuming the supporting foot is in static contact, we formulate the following equation balancing inertial, gravitational, and reaction moments [9]:

$$OP_k \times f_{r_k} + m_{r_k} = OS_k \times f_{s_k} + m_{s_k} - OG_k \times M_k g. \tag{1}$$

Here, G_k is the position of the center of gravity of the kth supporting extremity, M_k is the mass below the sensor point, and g is the gravitational acceleration vector. To compute the foot's CoP's, we consider the tangential part of the above equation with respect to the contact surface, i.e.,

$$\left[OP_k \times f_{r_k} = OS_k \times (f_{s_k} - M_k g) + m'_{s_k}\right]^{\mathcal{T}_k} \tag{2}$$

where

$$m'_{s_k} \triangleq m_{s_k} - S_k G_k \times M_k g \tag{3}$$

is a modified moment that includes the moment arm of the gravity at the sensor point, and the superscript $\mathcal{T}_k$ denotes tangential directions of the kth contact body. Note that m_{r_k} does not appear above because the definition of contact CoP implies zero tangential moments. Considering the force-balance equation

$$f_{r_k} = f_{s_k} - M_k g \tag{4}$$

we arrange (2) as

$$\left[(OP_k - OS_k) \times f_{r_k}\right]^{\mathcal{T}_k} = m'^{\mathcal{T}_k}_{s_k} \tag{5}$$

and solve it to get the CoP for the kth contact link as follows:

$$P_{kx} = S_{kx} - \frac{f_{r_{kx}}}{f_{r_{kz}}}\left(S_{kz} - P_{kz}\right) - \frac{m'_{sy}}{f_{r_{kz}}} \tag{6}$$

$$P_{ky} = S_{ky} - \frac{f_{r_{ky}}}{f_{r_{kz}}}\left(S_{kz} - P_{kz}\right) + \frac{m'_{sx}}{f_{r_{kz}}}. \tag{7}$$

Here, x and y refer to the tangential directions with respect to the local surface frames. The same analysis applies to the other extremities in contact, thereby defining the n_s contact CoP's.

To further characterize contact CoP's, we formulate the relationship between resultant moments at contact CoP's and reaction forces on contact bodies as follows:

$$m_{\text{cop}} \triangleq \begin{pmatrix} [m_{r1}]^{\mathcal{T}_1} \\ \vdots \\ [m_{rn_s}]^{\mathcal{T}_{n_s}} \end{pmatrix} = S_{\text{cop}}\, T_s\, F_r = 0 \quad \epsilon\, \mathcal{R}^{2n_s} \tag{8}$$

where F_r is the vector of reaction forces and moments projected onto the contact CoP's and expressed in global frame, i.e.,

$$F_r \triangleq \begin{pmatrix} f_{r1} \\ \vdots \\ f_{rn_s} \\ \hline m_{r1} \\ \vdots \\ m_{rn_s} \end{pmatrix} \epsilon\, \mathcal{R}^{6n_s} \tag{9}$$

where m_{cop} is the vector of tangential moments at contact CoP locations expressed in local frames, m_{rk} is the kth component of resultant moments, $\mathcal{T}_k$ indicates tangential components, T_s is a matrix that displaces moments from global frame to local surface frames, and S_{cop} is a selection matrix that selects tangential moments. Details on this matrices and on other matrices presented in this section are specified in the Appendix. Note that in (8), CoP conditions are modeled as zero tangential moments.

Characterizing contact CoP's is an important step toward developing contact models that describe intuitively the contact state of the robot. Based on these models, in the next section, we will develop methods that efficiently control the internal state of the robot. In particular, we will present control methods that allow us to manipulate contact CoP's to desired positions on the

contact surfaces. By manipulating contact CoP's away from contact edges, we ensure that contact surfaces stay flat against the supporting surfaces, thus avoiding undesired contact rotations. Additionally, controlling contact CoP's will result in compliant contact behaviors since they imply neutralizing tangential moments exerted by contact surfaces. The various properties of contact CoP's make them effective abstractions for the control and analysis of contact rotational behaviors.

B. Virtual-Linkage Model

We introduce a new instance of the virtual-linkage model [35] to describe the complex contact relationships formed between contact closed loops. The virtual-linkage model is a parallel multiarticulated mechanical model connecting closed loops between contact extremities using virtual prismatic and spherical joints. It was first used to describe the relationship between resultant and internal forces of a shared object between multiple manipulators. In the case of humanoids, the extremities in contact play the role of the manipulators, and the floor is the object with which to interact.

To design the virtual-linkage model for humanoid robots, we choose anchoring points located at the contact CoP positions that are defined previously. Therefore, contact CoP's act as the nodes connecting the linkages. To prevent supporting extremities from rotating along contact edges, our approach is to place contact CoP's as close as possible to the geometric centers of the extremities in contact. Hence, unwanted transitions to edge or point contacts will be avoided in case contact disturbances occur.

Note that placing contact CoP's at the centers of the links is not a necessary constraint. They can be placed at any position below the links in contact, but away from contact vertices and edges, to prevent rotations. Therefore, in this paper, we only consider flat-surface-contact interactions. Extensions to corner and edge contacts could also be explored using a similar methodology; however, we will leave this analysis open for the future.

We associate a virtual-linkage model connecting all contact CoP's. In the scenario, which is shown in Fig. 4, each body in contact introduces a tension with respect to its neighboring nodes as well as normal and tangential moments. For contacts with $n_s > 2$, we can independently specify $3(n_s - 2)$ tensions, n_s normal moments, and $2n_s$ tangential moments describing the CoP's. Any additional link in contact introduces three new tensions with respect to its neighbors and three more moments. No more than three tensions between neighboring nodes can be independently specified for a given contact. Internal tensions and normal moments characterize the behavior of contact bodies with respect to the friction cones and rotational friction properties of the surfaces in contact. The relationship between tension and reaction forces can be formulated as

$$f_t \triangleq \begin{pmatrix} \vdots \\ f_{tij} \\ \vdots \end{pmatrix} = S_t \; R_t \; \Delta_t \; F_r \quad \epsilon \, \mathcal{R}^{3(n_s-2)} \tag{10}$$

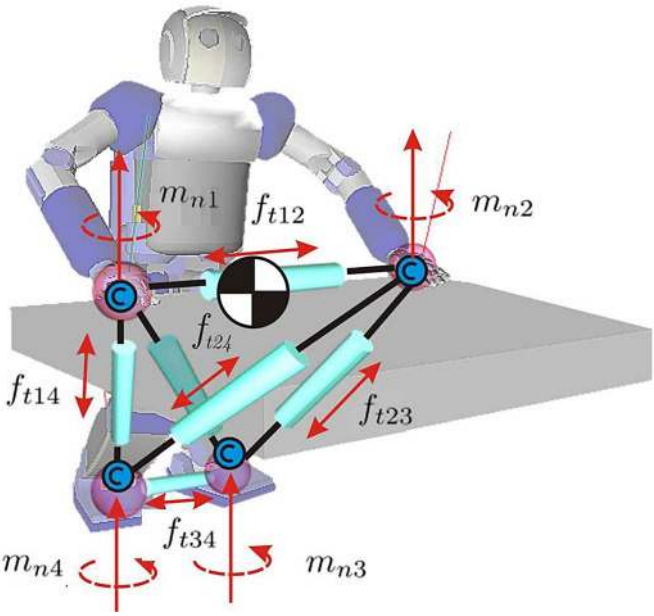

Fig. 4. Virtual-linkage model for humanoid robots. We define a virtual-linkage model anchored at the contact CoP's. It enables the characterization of internal tensions and moments against contact surfaces. The virtual-linkage model abstracts the behavior of internal and CoM forces with respect to reaction forces. These characteristics make the virtual-linkage model a powerful tool for the analysis and efficient control of CoM maneuvers and contact interactions.

where Δ_t is a differential operator matrix that differentiates pairs of tensions between contacts, R_t is the concatenation of rotation matrices from global frame to the directions uniting internal virtual-linkage nodes, and S_t is a selection matrix that chooses tension directions. Similarly, we characterize normal moments as

$$m_n \triangleq \begin{pmatrix} m_{n1} \\ m_{n2} \\ \vdots \\ m_{nn_s} \end{pmatrix} = S_n \; T_s \; F_r \quad \epsilon \, \mathcal{R}^{n_s} \tag{11}$$

where T_s is, once more, the matrix that displaces forces and moments to surface frames, and S_n is a selection matrix that chooses normal directions.

To complete the virtual-linkage model, we establish the relationship between resultant forces and moments acting on the robot's CoM with respect to contact reaction forces. The robot's CoM is an important variable because it characterizes the maneuverability of the robot to plan locomotion and weight-shifting behaviors. Similarly to the relationships developed in the original virtual-linkage model [35], we formulate the equations describing the balance of reaction forces and moments at contact bodies with respect to the resultant forces and moments taking place on the robot's CoM

$$\left(\begin{array}{ccc|ccc} [I]_{3\times3} & \cdots & [I]_{3\times3} & [0]_{3\times3} & \cdots & [0]_{3\times3} \\ \widehat{P}_1 & \cdots & \widehat{P}_n & [I]_{3\times3} & \cdots & [I]_{3\times3} \end{array}\right) F_r = \left(\begin{array}{c|c} [I]_{3\times3} & [0]_{3\times3} \\ \widehat{P}_{\text{com}} & [I]_{3\times3} \end{array}\right) F_{\text{com}} \tag{12}$$

where $[\hat{\cdot}]$ indicates the cross-product operator, P_i is the position of the ith contact CoP, $P_{\rm com}$ is the position of the CoM, and $F_{\rm com}$ is the 6-D vector of inertial and gravitational forces and moments at the robot's CoM. Combining (8) and (10)–(12), we obtain the following virtual-linkage model for humanoid robots:

$$\left(\frac{F_{\rm com}}{F_{\rm int}}\right) = GF_r \tag{13}$$

where $F_{\rm int}$ is the vector of internal forces and moments, which is defined as follows:

$$F_{\rm int} \triangleq \left(\frac{f_t}{\frac{m_{\rm cop}}{m_n}}\right) \epsilon\, \mathcal{R}^{6(n_s-1)} \tag{14}$$

and G is the grasp/contact matrix [35], which is defined as follows:

$$G \triangleq \left(\frac{W_{\rm com}}{W_{\rm int}}\right) \epsilon\, \mathcal{R}^{6n_s \times 6n_s} \tag{15}$$

with

$$W_{\rm com} \triangleq \left(\begin{array}{c|c} [I]_{3\times3} & [0]_{3\times3} \\ \hline \widehat{P}_{\rm com} & [I]_{3\times3} \end{array}\right)^{-1} \times \left(\begin{array}{ccc|ccc} [I]_{3\times3} & \cdots & [I]_{3\times3} & [0]_{3\times3} & \cdots & [0]_{3\times3} \\ \hline \widehat{P}_1 & \cdots & \widehat{P}_n & [I]_{3\times3} & \cdots & [I]_{3\times3} \end{array}\right) \epsilon\, \mathcal{R}^{6\times6n_s} \tag{16}$$

and

$$W_{\rm int} \triangleq \left(\frac{S_t\ R_t\ \Delta_t}{\frac{S_{\rm cop}\ T_s}{S_n\ T_s}}\right) \epsilon\, \mathcal{R}^{6(n_s-1)\times6n_s}. \tag{17}$$

The simultaneous planning and control of the positions of contact CoP's alongside with the behavior of the robot's CoM and the set of internal forces between contacts and normal surface moments is an intricate engineering problem. Such a problem involves characterizing the combined interactions between the above variables and finding solutions that fulfill unilateral contact constraints and friction properties of the contact surfaces.

The grasp/contact matrix presented in this section provides an intuitive representation of the dynamic and static interdependencies between those variables. As such, a solution to the problem of simultaneously maneuvering and interacting in an unstructured 3-D environment lies in querying the grasp/contact matrix to find feasible trajectories that fulfill contact constraints. A detailed discussion on the dependencies between CoM behavior and friction and unilateral contact constraints using the grasp/contact matrix is given in the Appendix.

In the next section, we will use the virtual-linkage model to create controllers that can govern internal force and CoM behaviors. We will later study the application of the grasp/contact matrix G to find solutions of CoM and internal-force behaviors that comply with rotational and frictional contact constraints.

III. Control of Contact Centers of Pressure and Internal Tensions/Moments

Here, we develop a controller that governs the positions of contact CoP's and tracks desired values of internal tensions and normal moments with respect to the supporting surfaces. We integrate this controller with our previous framework for whole-body prioritized control, unifying the control of constraints, CoM behavior, operational tasks, and internal forces.

A. Background on Whole-Body Control

Let us study the multicontact problem for n_s extremities in contact. The differential kinematics of contact points are represented as

$$\delta x_s \triangleq \left(\begin{array}{c} \delta x_{s(1)} \\ \vdots \\ \delta x_{s(n_s)} \end{array}\right) = J_s \left(\begin{array}{c} \delta x_b \\ \delta q \end{array}\right) \epsilon\, \mathcal{R}^{6n_s} \tag{18}$$

where $\delta x_{s(i)}\ \epsilon\ \mathcal{R}^6$ is the infinitesimal displacement of the contact CoP of the ith supporting extremity, $J_s\ \epsilon\ \mathcal{R}^{6n_s\times(6+n)}$ is the cumulative Jacobian of all contact CoP locations, δx_b and δq are the infinitesimal displacements of the robot's base and joint positions, n is the number of actuated joints, and $6+n$ represents the number of generalized coordinates that include the six underactuated joints describing the motion of the robot's base.

We used simple rigid contact models in [18] to derive estimates of reaction forces. With the premise that stable balance is maintained and that internal forces are controlled to keep the feet flat against the ground, we model contacts as rigid constraints, i.e.,

$$\vartheta_s = 0, \qquad \dot{\vartheta}_s = 0 \tag{19}$$

where ϑ_s is the time derivative of x_s. These constraints allowed us to derive the following simple model between contact forces and actuation torques [27]:

$$F_r = \overline{J}_s^T U^T \Gamma - \mu_r - p_r \tag{20}$$

where

$$\overline{J}_s \triangleq A^{-1} J_s^T (J_s A^{-1} J_s^T)^{-1} \tag{21}$$

$$\mu_r = \overline{J}_s b - \Lambda_s \dot{J}_s \left(\begin{array}{c} \vartheta_b \\ \dot{q} \end{array}\right) \tag{22}$$

$$p_r = \overline{J}_s g \tag{23}$$

are the dynamically consistent generalized inverse of the Jacobian [16] associated with contact CoP's, the Coriolis/centrifugal force term, and the gravitational force term, respectively. Additionally

$$U = \left(\begin{array}{cc} [0]_{n\times6} & [I]_{n\times n} \end{array}\right) \epsilon \mathcal{R}^{n\times(n+6)} \tag{24}$$

is the selection matrix of actuated quantities, and Γ is the $n\times1$ vector of actuation torques. We used this model in [22] to derive the following constrained whole-body equation of motion:

$$A \left(\begin{array}{c} \dot{\vartheta}_b \\ \ddot{q} \end{array}\right) + N_s^T (b+g) + J_s^T \Lambda_s \dot{J}_s \left(\begin{array}{c} \vartheta_b \\ \dot{q} \end{array}\right) = (UN_s)^T \Gamma \tag{25}$$

where A is the mass matrix involving the unactuated base and the actuated joints, ϑ_b is the vector of linear and angular velocities of the robot's base

$$N_s \triangleq I - \overline{J}_s J_s \tag{26}$$

is the dynamically consistent null space of the contact Jacobian, b and g are generalized Coriolis/centrifugal and gravity terms, and Λ_s is the $6n_s \times 6n_s$ mass matrix associated with all support contacts. The derivation of the above constrained equation of motion can be found in the Appendix.

To design an internal-force controller, we first analyze our previous framework for whole-body multitask control. We consider a vector of task descriptors given by

$$x \triangleq \begin{pmatrix} x_1 \\ \hline x_2 \\ \hline \vdots \\ \hline x_{n_t} \end{pmatrix} \tag{27}$$

where each x_k describes the coordinates of the kth control objective, and n_t is the number of task descriptors that are used to characterize the instantaneous behavior of the robot. Prioritized task kinematics can be expressed using joint velocities alone [27], i.e.,

$$\dot{x}_k = J_k \begin{pmatrix} \vartheta_b \\ \dot{q} \end{pmatrix} = J_k \, \overline{UN_s} \, \dot{q} \tag{28}$$

where $J_k \, \epsilon \, \mathcal{R}^{m_k \times (n+6)}$ is the Jacobian of the m_kth-dimensional coordinate x_k with respect to the inertial frame of reference and $\overline{UN_s}$ is the dynamically weighted generalized inverse of UN_s. The term $J_k \overline{UN_s}$ acts as a constrained Jacobian, which maps joint velocities into task velocities. We refer to it using the symbol

$$J_k^* \triangleq J_k \overline{UN_s} \quad \epsilon \, \mathcal{R}^{m_k \times n}. \tag{29}$$

The above model is general for arbitrary contact situations. When the contact stance changes, (26) changes to reflect the new stance coordinates, and therefore, the models of (25) and (28) change too. For instance, the example involving cleaning a side panel shown in Fig. 6, involves switching from a biped stance, to a four-point multicontact, and finally, to a three-point multicontact stance. Consequently, the contact models for the different phases need to be changed when there occurs a new contact event.

To simultaneously optimize all task objectives, we implement prioritized torque controllers under multicontact and underactuation constraints, as described in [27], and characterized by the global torque vector

$$\Gamma = \sum_{k=1}^{N} \left(J_{k|\mathrm{prec}(k)}^{*T} F_k \right) + N_t^{*T} \Gamma_{\mathrm{posture}} \tag{30}$$

where $J_{k|\mathrm{prec}(k)}^*$ are prioritized Jacobians, F_k are dynamically consistent control forces, N_t^* is the cumulative prioritized null-space matrix associated with higher priority tasks, and $\Gamma_{\mathrm{posture}}$ is a postural control vector that operates in the null space of all tasks. We proposed prioritization in [27] to unify the control of CoM behavior, geometric constraints, operational tasks, and postural behavior. This unification process led to the following whole-body torque-control representation for humanoid robots:

$$\begin{aligned} \Gamma = {} & J_c^{*T} F_c + J_{\mathrm{com}|c}^{*T} F_{\mathrm{com}} \\ & + J_{t|\mathrm{com}|c}^{*T} F_{\mathrm{tasks}} + J_{p|t|\mathrm{com}|c}^{*T} F_{\mathrm{postures}}. \end{aligned} \tag{31}$$

where the subscripts followed by $|$ indicate prioritization, and the symbols c, t, and p denote constraints, tasks, and postures, respectively. The command F_{com} is a vector of control forces to maneuver the robot's CoM behavior. CoM stability behavior and control will be analyzed in more detail in the following sections.

B. Manifold of Internal Forces

We define the space of internal-force behavior as the torque components that have no effect on the robot's motion, i.e., that produce zero accelerations on the robot's base or on the actuated joints. This condition can be modeled by analyzing the right-hand side (RHS) of (25), thus leading to the following expression:

$$(UN_s)^T \Gamma = 0 \tag{32}$$

which reflects the cancelation of acceleration effects. Therefore, the torques that fulfill the above constraint belong to the null space of (UN_s), which is defined by the projection

$$L^* \triangleq \left(I - UN_s \, \overline{UN}_s \right) \epsilon \mathcal{R}^{n \times n} \tag{33}$$

where we use the symbol L^* to denote contact closed loops, and the superscript * to indicate that the projection operates in contact space. The torques associated with internal forces are those that do not contribute to net movement, i.e.,

$$\Gamma = L^{*T} \Gamma_{\mathrm{int}} \tag{34}$$

where Γ_{int} denotes the control input to control internal forces and moments. Note that plugging the above torques in the RHS of (25) cancels out Γ_{int}, thus fulfilling the cancelation of acceleration effects.

C. Whole-Body Controller With Internal-Force Command

We integrate the above torques with our prioritized controller discussed in (30), leading to the following unified torque structure:

$$\Gamma = \sum_{k=1}^{N} \left(J_{k|\mathrm{prec}(k)}^{*T} F_k \right) + N_t^{*T} \Gamma_{\mathrm{posture}} + L^{*T} \Gamma_{\mathrm{int}}. \tag{35}$$

The next step consists of using the above structure to control internal-force behavior, as characterized in (14), to desired reference values, i.e.,

$$F_{\mathrm{int}} \longrightarrow F_{\mathrm{int,ref}} = \begin{pmatrix} f_{t,\mathrm{ref}} \\ \hline [0]_{2n_s} \\ \hline m_{n,\mathrm{ref}} \end{pmatrix}. \tag{36}$$

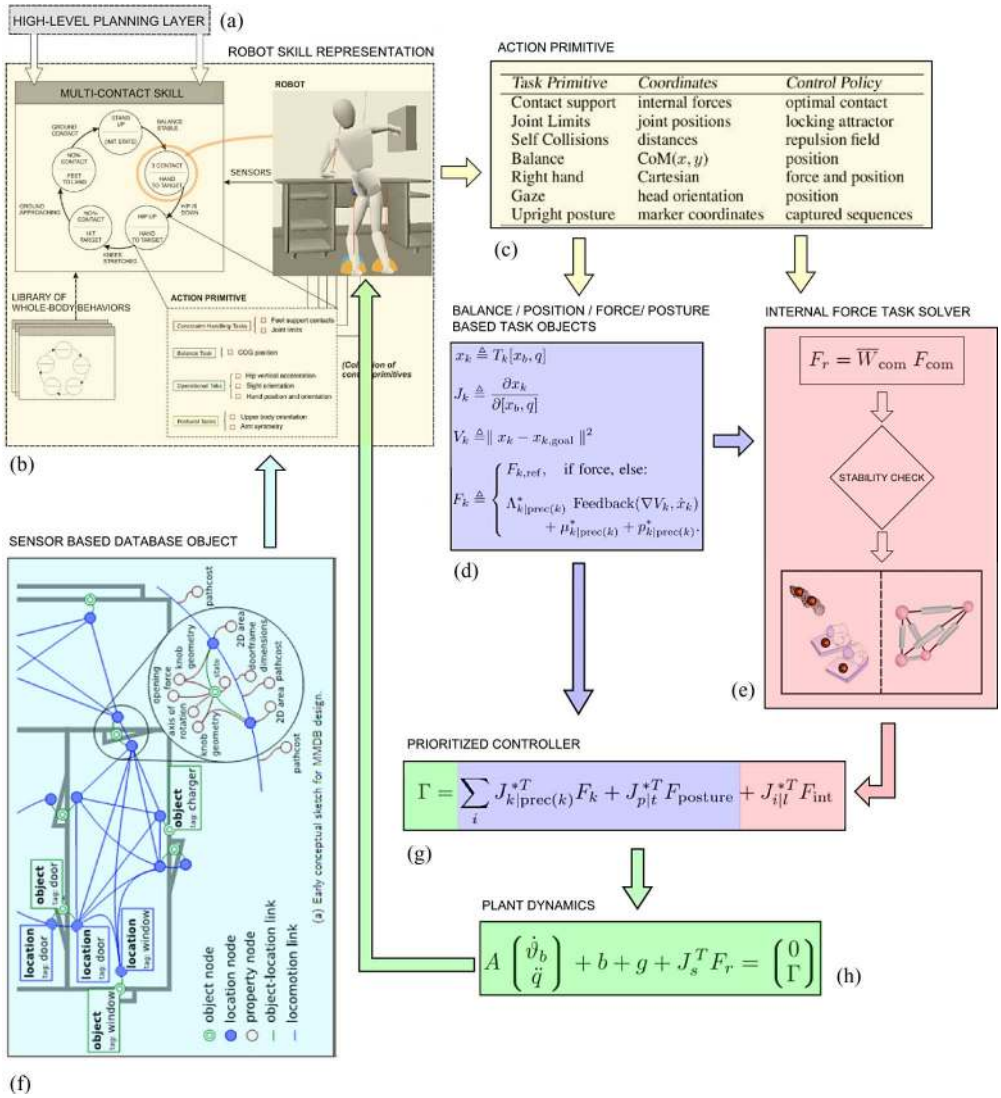

Fig. 5. Whole-body torque controller. (a) Decisions made by a high-level-planning module, such as the decision module presented in [23]. (b) Outlines the information contained in behavioral entities representing the desired skills; here, it is depicted for a multiphase multicontact behavior. These entities are defined by state machines where the states consist of action primitives. Behavior primitives received information from a sensor-based database that is used to update the action states and their representations. (c) Description of action primitives as collections of task objects organized according to a desired priority ordering. The action primitive shown above corresponds to one of the states of the desired multicontact behavior. (d) Task objects as entities containing coordinate representations, differential kinematic representations, goal-based potential functions, and force-based control policies. (e) System currently under development that is used to automatically solve internal-force behavior given a desired action representation. This module is not described in this paper. (g) Prioritized torque-based controller, which uses the previous behavior representations and control policies to create whole-body control torques. (h) Estimated dynamic behavior of the underactuated robot under multicontact constraints in response to the previous torque commands.

These reference values are planned to fulfill frictional constraints of the surfaces in contact using planning techniques, such as the one mentioned in the controller of Fig. 5 (which is now under development).

To do that, we design a new torque controller that can directly manipulate internal-force behavior. We first note that the virtual-linkage model, which is derived in (13) and (15), leads to the following relationship between internal forces with respect to contact forces:

$$F_{\text{int}} = W_{\text{int}} F_r. \tag{37}$$

Substituting the proposed whole-body-torque command of (35) into (20), and using (37), we obtain an equality that relates internal-force behavior with respect to internal-torque commands, i.e.,

$$F_{\text{int}} = \overline{J}^{*T}_{i|l}\, \Gamma_{\text{int}} + F_{\text{int},\{t,p\}} - \mu_i - p_i \tag{38}$$

where

$$\overline{J}^{*}_{i|l} \triangleq \left(L^* U \overline{J}_s W^T_{\text{int}} \right) \tag{39}$$

is a transformation matrix from torques to forces

$$F_{\text{int},\{t,p\}} \triangleq W_{\text{int}} \overline{J}_s^T U^T \left[\sum_{k=1}^{N} \left(J^{*T}_{k|\text{prec}(k)} F_k \right) + N_t^{*T} \Gamma_{\text{posture}} \right] \tag{40}$$

are forces induced by task and postural behavior, and μ_i and p_i are Coriolis/centrifugal and gravity terms defined as

$$\mu_i \triangleq W_{\text{int}}\mu_r, \qquad p_i \triangleq W_{\text{int}}p_r. \tag{41}$$

Note that the above terms result in task and postural torques appearing twice in the command torque of (35). However, (40) does not interfere with task and postural behavior, since it operates in the manifold of closed loops. This term is meant to cancel out task and postural components introduced in the close-loop contact behavior.

Inverting (38), we derive the desired torque-based internal-force controller given by

$$\Gamma_{\text{int}} = J_{i|l}^{*T}\left(F_{\text{int,ref}} - F_{\text{int},\{t,p\}} + \mu_i + p_i\right) \tag{42}$$

where $J_{i|l}^{*}$ is a Moore–Penrose left-pseudoinverse of (39), and the subscript $\{i|l\}$ denotes internal quantities operating in the space of contact closed loops. Substituting the above expression into (38) and provided that $J_{i|l}^{*}$ is full row rank, we obtain the linear equality given by

$$F_{\text{int}} = F_{\text{int,ref}}. \tag{43}$$

To ensure that $J_{i|l}^{*}$ is full row rank, L^{*} needs to span all internal-force and moment quantities. This applies if there are at least six independent mechanical joints separating the common ancestors between contact closed loops. A second required condition is to ensure that W_{int} defines independent internal quantities. This is already ensured in our derivation of the virtual-linkage model.

Although the above controller will work in open loop, to achieve accurate tracking of internal forces under actuator friction and mechanical modeling errors, a feedback force-control law involving proportional–integral–derivative feedback (PID) is needed. Given appropriate choice of the control law, the above linear relationship will ensure convergence to the desired internal-force trajectories.

The above control structure provides a dynamically correct internal-force controller that has no coupling effects on task, CoM, and postural behaviors, thereby enabling the efficient control of whole-body multicontact interactions. It provides the support to simultaneously control the position of multiple contact CoP's and the internal tensions and normal moments acting between contact closed loops. A block diagram of the overall whole-body torque controller with internal force commands is shown in Fig. 5.

D. Boundaries of Center-of-Mass and Internal-Force Behavior

The control of CoM and internal-force behavior is directly related to the friction properties of the supporting surfaces. Here, we analyze this relationship and the effect on contact stability with respect to surface-friction boundaries. The torque command of (35) entails controlling both the robot's CoM and the internal-force behaviors. As discussed in (31), CoM behavior is always one of the task objectives involve in the torque reference of a humanoid robot.

The trajectory and values of CoM and internal-force behavior cannot take arbitrary values. They need to be chosen to fulfill contact and frictional constraints at the supporting surfaces. Ensuring that reaction forces remain within friction boundaries is required to prevent robot contact extremities from sliding and rotating with respect to the environment.

To facilitate the analysis of friction behaviors with respect to surface properties, we rotate reaction forces and moments, which are normally expressed in global frame, as shown in (20), to align with the frames attached to the contact surfaces; therefore, their z-components are parallel to surface normals, i.e.,

$$F_{\text{surf}} \triangleq R_{\text{surf}}\ F_r. \tag{44}$$

Here, F_{surf} represents the rotated forces and moments, and R_{surf} is a $6n_s \times 6n_s$ rotation matrix that aligns z-components to surface normals. Using the above transformation, (13) can be written as

$$\begin{pmatrix} F_{\text{com}} \\ \hline F_{\text{int}} \end{pmatrix} = GR_{\text{surf}}^{-1}F_{\text{surf}} \tag{45}$$

where

$$F_{\text{com}} \triangleq \begin{pmatrix} f_{\text{com}} \\ m_{\text{com}} \end{pmatrix}, \qquad F_{\text{int}} \triangleq \begin{pmatrix} f_{\text{int}} \\ m_{\text{int}} \end{pmatrix} \tag{46}$$

are the forces associated with the robot's CoM and internal-force behaviors, and R_{surf}^{-1} is an inverse cumulative rotation. The above expression can be used to estimate the surface forces due to CoM and internal-force commands, i.e.,

$$F_{\text{surf}} = R_{\text{surf}}G^{-1}\begin{pmatrix} F_{\text{com,ref}} \\ \hline F_{\text{int,ref}} \end{pmatrix}. \tag{47}$$

Using the above expression, we can analyze the stability of whole-body behaviors with respect to frictional properties of the contact surfaces. We consider the following indexes associated with linear frictional cones and rotational frictional ratios for the kth contact extremity:

$$\alpha_{\text{surf},k} \triangleq \begin{pmatrix} \tan^{-1}\left(\frac{f_{\text{surf},kz}}{f_{\text{surf},kx}}\right) \\ \tan^{-1}\left(\frac{f_{\text{surf},kz}}{f_{\text{surf},ky}}\right) \end{pmatrix} \tag{48}$$

$$\beta_{\text{surf},k} \triangleq \frac{m_{\text{surf},kz}}{f_{\text{surf},kz}} \tag{49}$$

where $\alpha_{\text{surf},k}$ is the vector of angles measured between the surface plane and the reaction-force vector, and $\beta_{\text{surf},k}$ is a ratio between the normal moment and normal force that characterizes the rotational friction behavior. This last index provides an intuitive metric of rotational friction characteristics since it normalizes normal moments with respect to normal forces. We determine the boundaries of the above indexes by using simple models involving static friction cones and a heuristic model for rotational friction, i.e.,

$$\alpha_{\text{surf},k}\ \epsilon\ \text{fricCone}(k) \tag{50}$$

$$\beta_{\text{surf},k}\ \epsilon\ \text{rotIndex}(k). \tag{51}$$

On the other hand, the boundaries of CoP locations are determined by the surfaces in contact, i.e.,

$$P_k \, \epsilon \, \mathrm{surfArea}(k) \tag{52}$$

where P_k are contact CoP's and $\mathrm{surfArea}(k)$ is the surface area of the contact bodies. Overall, (50)–(52) determine the boundaries of frictional and rotational stability that comply with the contact model defined in (19).

As we mentioned earlier, we control contact CoP's to be located close to contact geometric centers. The choice of CoP's defines the anchors of the virtual-linkage model and, therefore, determines the model of the grasp/contact matrix. Once G is defined, we use the boundaries defined in (50)–(52) to obtain feasible values of CoM and internal forces by means of (47). The problem of choosing internal force and CoM behavior is analyzed in more detail in the simulations section and in the Appendix.

IV. Simulation Results

We now study various experiments on a simulated model of Asimo demonstrating the capabilities of the above methods. The objective of Asimo is to operate in offices and homes, thereby assisting humans in a variety of service and care-giving chores. Recently, we have developed a research version of Asimo that uses torque-control commands [19]. Torque-control robots have the ability to implement compliant behaviors, which is needed to operate effectively and safely in human environments. The objective of this section is to demonstrate the ability to control contact CoP's, internal forces, and CoM behavior using the proposed methods.

A dynamic simulation environment [4] and a contact solver based on propagation of forces and impacts [26] are used to simulate the execution of our methods. The whole-body controller described in (35) is implemented on a task-based software environment that enables the online creation of whole-body behaviors. Using this environment, we create various behaviors involving biped and multicontact stance, as well as operational space interactions and CoM maneuvers.

A. Simulation of Reaching and Cleaning a Panel

In the experiment shown in Fig. 6, we implement a multicontact behavior that involves the following steps:

1) moving the robot's hands toward a table;
2) establishing four-contact support and moving the robot's CoM toward the table to reach further away;
3) transitioning to three contacts by displacing the CoM above the convex hull formed by the feet and left hand;
4) placing the right hand on the side panel for interactive manipulation.

This sequence of actions is accomplished using a state machine, where each state involves optimizing multiple low-level task objectives. Once in contact, the robot's right hand is commanded to exert a normal force of 60 N perpendicular to the side panel while tracking a trajectory tangential to the panel and commanded by a user. To add more complexity to the skill, we command the CoM vertical behavior to move up and down in a sinusoidal pattern. To achieve the desired global behavior, we simultaneously control the robot's CoM, several operational tasks, and postural behaviors, as indicated in (31) (for more details, see [27]), as well as the internal-force-control policy, as defined in (42). Using (13), we construct three virtual-linkage models for the phases involving two, three, and four contacts. For simplicity, all tension forces and normal moments are controlled to become zero. For instance, for the phase with three-support contacts, the vector of internal-force commands is given by

$$F_{\mathrm{int}} \longrightarrow F_{\mathrm{int,ref}} = [0]_{12}. \tag{53}$$

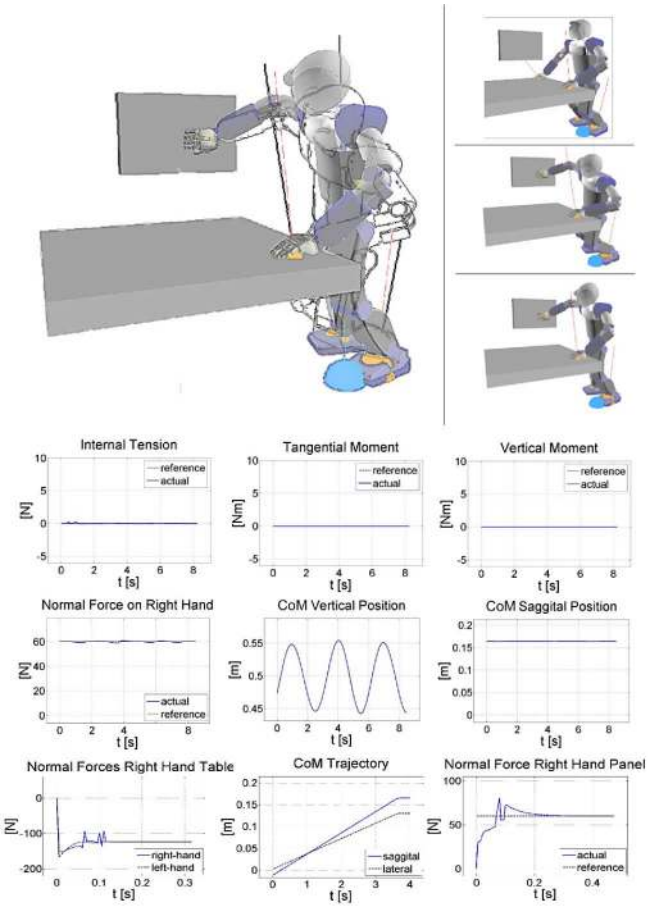

Fig. 6. Unified whole-body multicontact behavior with internal-force and moment control. The robot is supported on its legs and left hand, while the right hand exerts a normal force of 60 N against the panel while tracking a teleoperated trajectory tangential to the plane. The CoM is commanded to follow a sinusoidal vertical trajectory while its horizontal behavior remains fixed. Contact CoP's are controlled to remain at the geometric center of contact bodies, and internal tensions and normal moments are controlled to become null. The data graphs show good tracking on the various control parameters. The top two rows show data when the robot is supported with the left hand and the two feet. It shows moment values on the left-supporting hand and its tension force with respect to the right foot. It also shows force tracking on the right panel and CoM trajectory tracking. The lower row shows data for diverse transitions. As shown on the small top-right images, the robot transitions from biped stance, to four-contact support and, finally, to three-contact support. The lower graphs show first the force value when the right hand makes first contact with the supporting table. It then shows the trajectory of the CoM in the sagittal direction when the robot shifts weight toward the support area defined by the left hand and the two feet. Finally, it shows the transition forces when the right hand makes first contact with the side panel.

The position of contact CoP's on hands and feet is chosen to be at the geometric center of the links in contact.

During the bipedal phase, the CoM is commanded to stay between the feet while moving the hands toward the table, while CoM and CoP positions are controlled taking into account the bipedal dependencies, which are analyzed in the Appendix in (74). In the phases with four contacts, the CoM is commanded to maneuver toward the table by tracking a trajectory that fulfills contact-stability constraint, as defined by the boundaries of (50)–(52). This trajectory is discussed in detail later in this section. A feedback controller to track this trajectory is implemented using force commands in CoM space. The control of the right hand to interact with the side panel is implemented using the force-control methods, as described in [22]. Therefore, a unified force/position operational task is created to control the right hand. Postural behavior is controlled by optimizing a criterion that minimizes the distance with respect to a human prerecorded posture using a method similar to the one described in [7]. During the multicontact phases (i.e., three or more supporting contacts) virtual-linkage models similar to that shown in Fig. 4 are implemented. During the biped phase, the special case of virtual-linkage model, as discussed in Fig. 11 in the Appendix, is used. Details on the algebraic expressions of the matrices involved in the virtual-linkage models are also given in the Appendix.

The first two rows of the accompanying data correspond to the phase with three supporting contacts, where the right hand is controlled to clean the panel. In this phase, the horizontal position of the CoM is commanded to remain fixed. We display data on the tension forces occurring on the virtual-linkage model assigned between the left hand and the right foot, the moments about the CoP on the left hand, the normal force on the panel, and the sagittal and vertical trajectories of the CoM. As we observe, the whole-body controller with internal-force control is able to efficiently track the desired internal-force values as well as the desired operational task commands involving the right hand and CoM. Although it is not shown here, all other internal tensions and moments are able to track the desired values with high accuracy. In fact, to add noise to the simulation, we have applied some unmodeled external forces to the robot's body. Otherwise, the tracking performance would have been unrealistically good. On the bottom row of data, we show normal forces on the table when establishing contact with the hands, the CoM horizontal trajectories used to move the robot's body closer to the table once four contacts are established, and the normal forces on the panel when the first impact occurs.

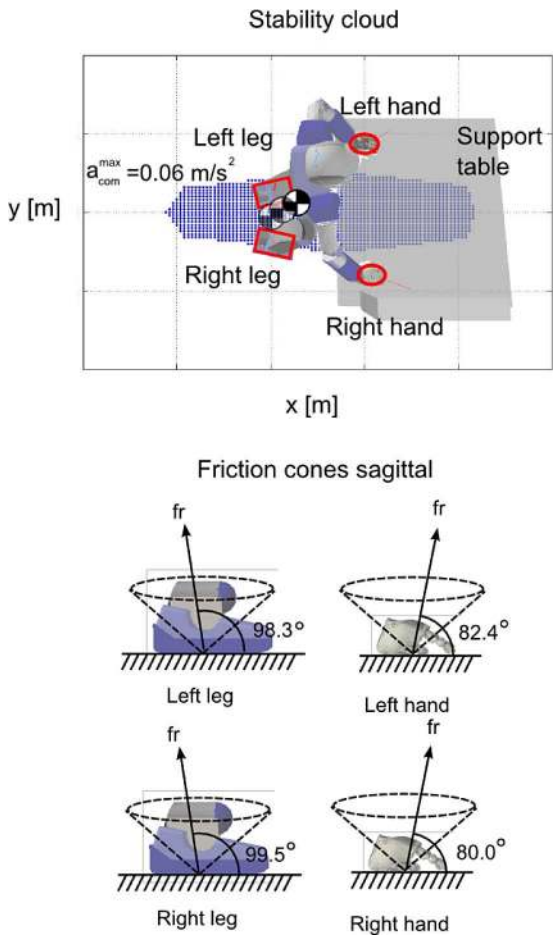

Fig. 7. Analysis of CoM behavior. The top image depicts the stability cloud of feasible CoM static positions given frictional constraints. The CoM trajectory, which must start and finish within the stability cloud, is overlaid. Maximum accelerations and decelerations are limited to 0.06 m/s^2 to remain within frictional cones. The lower part of the figure depicts frictional cones with respect to the contact surfaces in the sagittal directions and the reaction forces (within limits) during peak decelerations.

B. Design of Center-of-Mass Behavior

During the simulation shown in Fig. 6, the robot places the hands on the table and establishes support by moving its CoM from the center of the feet to the final position closer to the table, as shown in Fig. 7. By supporting its body with the hands on the table, the robot is able to reach the far away areas of the panel that need to be cleaned. We focus our attention on the behavior of the CoM during the support maneuver. There are two critical components that need to be studied to plan a stable CoM maneuver: the feasible area of CoM static positions and the feasible CoM accelerations with respect to the frictional properties of the terrain and with respect to unilateral contact constraints.

To analyze the stability region, we exploit the properties of the grasp/contact matrix. The grasp/contact matrix, as expressed in (16) and (17), depends only on the position of the robot's CoM and on the positions of the contact CoP's, i.e.,

$$G = \text{func}\left(P_{\text{com}},\ P1,\ \ldots,\ P4\right) \tag{54}$$

where func stands for function. We also note that the vector of forces and moments at the CoM depends on inertial and gravitational accelerations as follows:

$$F_{\text{com}} \triangleq \begin{pmatrix} f_{\text{com}} \\ m_{\text{com}} \end{pmatrix} = \begin{pmatrix} M\left(g + a_{\text{com}}\right) \\ \sum_{i=1}^{n}\left[I_{\text{com}(i)}\ \alpha_{\text{com}(i)} + p_{\text{com}(i)} \times \left(m_i\ a_{\text{com}(i)}\right)\right] \end{pmatrix} \tag{55}$$

where M is the total mass of the robot, $a_{\rm com}$ is the vector of linear accelerations of the robot's CoM, g is the gravitational acceleration vector, $I_{{\rm com}(i)}$ is the inertial tensor of the ith link expressed at its CoM, $p_{{\rm com}(i)}$ is its CoM position, m_i is its mass, $\alpha_{{\rm com}(i)}$ is the vector of angular accelerations, and $a_{{\rm com}(i)}$ is the vector of linear accelerations.

Our technique consists of scanning the G matrix for an array (i.e., cloud) of CoM points around the robot's multicontact area and then evaluating if these points, which translate into gravitational forces in the static case, fulfill frictional constraints, as expressed in (50) and (51). To evaluate the feasibility, we use the model described in (47). The stability cloud is shown in Fig. 7. The CoM-feasible placements that comply with the stance's frictional characteristics are shown as shaded dots.

The above stability area is used to plan initial and final CoM positions that need to lie on top of the static stability area. The dynamic trajectory of the robot's CoM is then planned within this region (which is shown in the bottom graph of Fig. 6). Here, we have designed a CoM trajectory with constant velocity throughout most of the displacement, and with an acceleration and deceleration profile obtained using trigonometric curves. The profile of the acceleration and deceleration does not exceed values higher than 0.06 m/s^2. To verify that this profile is feasible with respect to frictional constraints, we use (55) to convert accelerations into CoM forces (for simplicity, we ignore CoM moments). We then use (47) to validate the feasibility of the trajectory. At the bottom of Fig. 7, we show the reaction forces that are induced by the peak-deceleration profile, which occurs close to the very end of the CoM displacement, when $p_{\rm com} = [0.16,\ 0.13,\ 0.47]$. As we can observe, the orientation of the reaction forces is within the limits of the frictional cones, which is shown here in the sagittal directions. The same analysis has been carried out with respect to lateral frictional characteristics as well as with respect to rotational friction constraints on the discussed simulation.

C. Design of Control Laws

In Fig. 5, we depicted a diagram of our whole-body controller expressing behaviors as state machines, where each state (which is called action primitive) is a collection of low-level task primitives. In turn, each task primitive optimizes an objective either using potential fields or force control.

We focus our attention on the action primitive involved in the phase of cleaning the panel. The objectives being controlled here are summarized in the following table.

Task Primitive	*Coordinates*	*Control Policy*
Balance	CoM	dynamic trajectory
Right hand	Cartesian	force and position
Gaze	head orientation	position
Posture	marker coordinates	captured sequences
Internal forces	tensions / moments	optimal contact

Task objectives are controlled using the prioritized structure shown in (35). In the case of CoM trajectory control, the controller involves calculating the CoM Jacobian, which can be derived using the following expressions:

$$J_{\rm com} \triangleq \frac{1}{M}\sum_{i=1}^{n} m_i J_{{\rm com}(i)} \tag{56}$$

where

$$J_{\rm com(i)} \triangleq \begin{pmatrix} \dfrac{\partial x_{{\rm com}(i)}}{\partial x_b} \\ \dfrac{\partial x_{{\rm com}(i)}}{\partial q} \end{pmatrix} \epsilon\, \mathcal{R}^{2\times(n+6)} \tag{57}$$

is the Jacobian for the ith contact link.

As discussed in [27], trajectory tracking involves calculating dynamically consistent forces described by the following equation:

$$F_{\rm com} = \Lambda^*_{\rm com}\, a_{\rm com,ref} + \mu^*_{\rm com} + p^*_{\rm com} \tag{58}$$

where $\Lambda^*_{\rm com}$ is the constrained mass matrix of the robot's CoM, $\mu^*_{\rm com}$ are forces induced by Coriolis/centrifugal effects, $p^*_{\rm com}$ are forces induced by gravity effects, and $a_{\rm com,ref}$ is the command acceleration vector. For the case of CoM control, we use the following feedback proportional/derivative tracking law:

$$a_{\rm com,ref} = -k_p\,(x_{\rm com} - x_{\rm des}) - k_v\,(\dot{x}_{\rm com} - v_{\rm des}) \tag{59}$$

where the position and velocity trajectories are designed following the feasible CoM profile discussed previously.

We also consider the control policy for the right hand in contact with the side panel. Here, we use a unified force-motion task defined by the law

$$\begin{aligned} F_{\rm hand} = \Omega_f \Bigg[& -K_{pf}\,(F_{x,\rm hand} - F_{\rm des}) - K_{vf}\dot{F}_{s,\rm hand} \\ & - K_{if}\int_0^t (F_{x,\rm hand} - F_{\rm des})\,dt \Bigg] \\ & + \Omega_m \Big[K_{vm}\,(\dot{x}_{\rm hand} - \nu v_{\rm des}) \Big] \end{aligned} \tag{60}$$

where $F_{s,\rm hand}$ are forces sensed at the hand. The above equation involves a PID control law to control the force in the normal direction defined by the projection Ω_f and a term to control the motion in the tangential directions to the panel defined by the projection Ω_m. The motion-control law is a velocity-saturation law defined by the position-feedback rule given by

$$v_{\rm des} = -K_{pm}\,K_{vm}^{-1}\,(x_{\rm hand} - x_{\rm des}) \tag{61}$$

with

$$\nu = \min\left\{1,\ \frac{v_{\max}}{\parallel v_{\rm des} \parallel}\right\}. \tag{62}$$

This ensures that we track user-defined trajectories without violating predefined velocity limits. To respond compliantly to impacts, we use moderate gains in the above motion-control law. In Fig. 6, we show the response to impact with the panel and with the table when establishing the contact interactions.

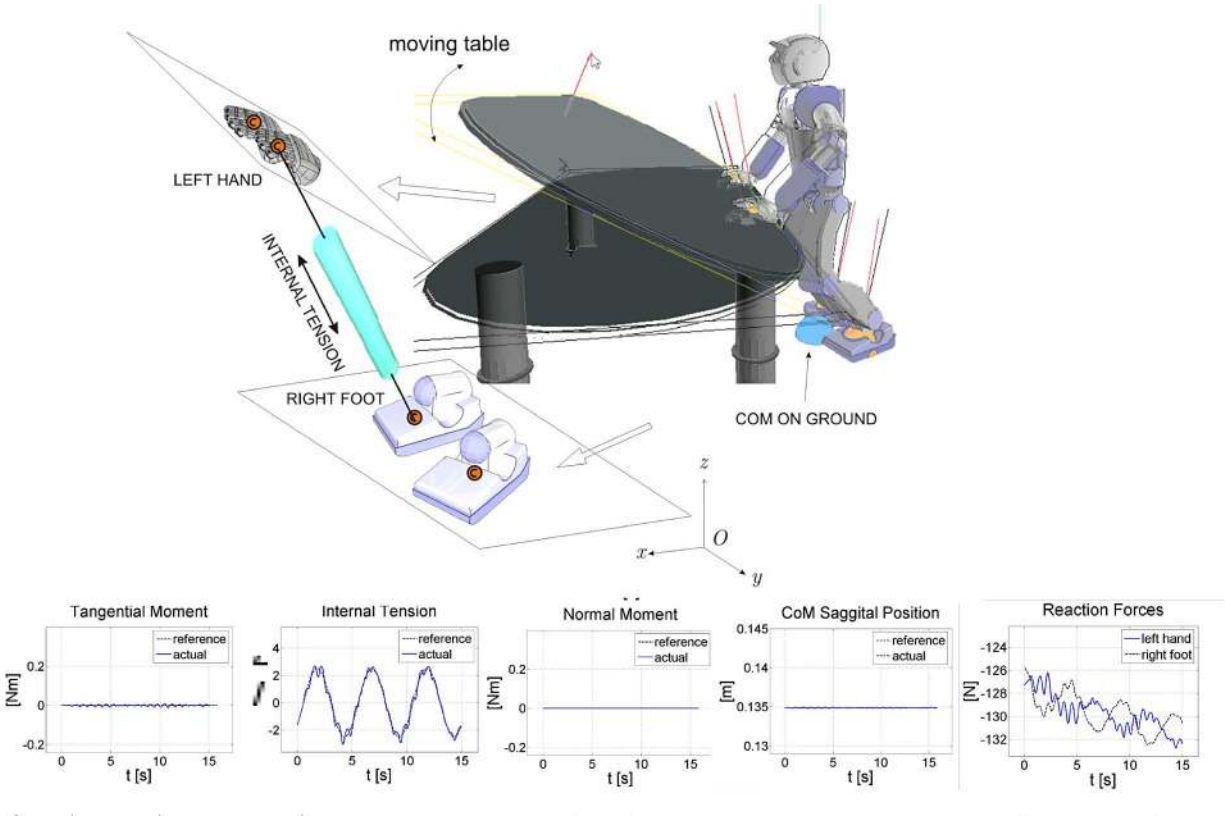

Fig. 8. Compliant multicontact behavior. A four-contact stance is shown here. Contact CoP's are controlled to stay at the center of the bodies in contact. The CoM is controlled to remain at a fixed location over the area defined by the horizontal projection of the four contacts. The table is pivoted rapidly by an external user to challenge the pose. To add additional difficulty, the internal tension between the left hand and the right foot is commanded to track a sinusoidal trajectory. All other tensions and normal moments are commanded to become null. Overall, the robot was able to track efficiently the commanded internal force and moment references with maximum errors around 0.3 N. We show the data corresponding to the left hand, including the tangential moments on the y-direction, the internal tension between the right hand and the left hand, and the normal moment with respect to the moving surface. As we can see, the tangential moment is maintained close to zero, which means that the desired anchor point of the virtual linkage, which, in our case, is the center of the hand, becomes the actual CoP. The tensions are also tracked efficiently as well as the normal moment. We also show data of the robot's CoM and the normal component of the reaction forces in the hands produced by the moving table. The desired CoM position was tracked with offset values below 0.1 mm, despite the large variation on the movement of the table that oscillated to angles up to 75° from the resting position.

D. Simulation of a Compliant Multicontact Behavior

We conduct a second simulation shown in Fig. 8 that studies a compliant behavior that emerges when the environment is dynamically moving. The robot is commanded to establish a four-contact stance leaning against a pivoting table. The tasks used to implement this behavior are similar to the ones used in the previous example; however, the robot is commanded to stay in the four-contact stance all the time. To demonstrate force tracking at the internal level, the tension between the left hand and the right foot is commanded to follow a sinusoidal trajectory. All other internal forces and tensions are commanded to be zero. At the same time, a user interacts with the pivoting table moving it up and down in arbitrary fast motions.

Because contact CoP's are commanded to stay at the center of the extremities in contact, the hands respond compliantly to table movement, remaining flat against the surface to maintain the desired CoP positions. The accompanying data graphs show tangential and normal moments, the tension between the left hand and the right foot, and the sagittal position of the CoM. We also show the normal component of the reaction forces induced by the table movement on the hands. The tracking error for the internal tension is small with a maximum excursion of 0.3 N. This error is mainly caused due to the unmodeled movement of the table. As we recall, our framework assumes that the table is static, which is implied in (19). However, because the table undergoes fast accelerations, the model is inaccurate. Despite this inaccuracy, the tracking behavior is very good. When the tabletop remains static, the force-tracking error is nearly zero (not shown here).

E. Discussion of Results

The most important result in the above simulations is the emergence of compliant interactions with respect to the dynamic environment while optimizing task objectives. While the robot is supporting its body against the table and floor, it is adapting to large variations on the orientation of the table. Compliance emerges because the behaviors are controlled using force and moment control as opposed to position-control strategies. The CoP's in the hands and feet are controlled to remain at the center of the surfaces in contact. This is achieved by creating a virtual-linkage model anchored at the center of the extremities and controlling the tangential moments to become zero. Because the

tangential moments in all four extremities remain close to zero, the hands respond compliantly to the disturbances produced by the table movement.

The internal tensions are tracked as expected, following the desired trajectories with small errors. These errors appear due to the unmodeled movement of the table. In the case of our simulation, we use open-loop control of the internal tensions. However, by using a PID control strategy, the dynamic response of the tension behavior might be improved. In real robots, it would be best to use a PID control strategy to overcome model errors and unmodeled actuator friction. However, using an integration feedback term can lead to large accumulation of error if the extremities lose contact accidentally. In such a case, the integral part might continuously increase the commanded force due to the lack of contact sensory feedback. Therefore, special care needs to be taken to avoid these types of accidents. In both simulations above, the CoM behavior tracks the desired values with high accuracy. This is accomplished due to the decoupling effect of the contact closed-loop operator discussed in (33).

An important discussion is the effect on the controller due to uncertainties in the model, actuators, and environment. The unmodeled uncertainties of the moving environment are handled by the compliance that emerges due to the use of the proposed internal-force controller. To overcome the effects on unmodeled friction at the joints due to the the gearing mechanisms, we use sensor-based PID control in the internal-force tracking tasks. We have conducted simulations that involved large modeling errors on the estimated link masses, inertias, and CoM locations. We evaluated the performance of an operational task involving tracking an end-effector trajectory while keeping balance on a standing posture, observing that the commanded whole-body behaviors remained stable, despite large deviations on the model. The most visible effects were in postural deviations due to the uncertainty on CoM estimation.

V. Conclusion

Creating a virtual-linkage model for humanoid robots enables the characterization of complex whole-body multicontact interactions and the creation of new compliant skills needed to operate effectively in human environments. By enabling the precise control of contact CoP's, we create compliant contact behaviors, and by placing contact CoP's near the center of contact bodies, we prevent unwanted rotations along contact edges. Characterizing the behavior of internal tensions and moments as well as the behavior of the robot's CoM with respect to contact reaction forces, we provide tools to plan policies that satisfy all frictional constraints. Other methods solely based on ZMP modeling disregard the local interactions between contact bodies hindering the ability to comply with contact constraints and to create compliant contact behaviors. Our methods are dynamically correct, enabling the simultaneous control of operational tasks, CoM behavior, postures, and internal forces with high accuracy. We have demonstrated these capabilities through whole-body multicontact simulations of the humanoid robot Asimo.

Suggestions for future work include the implementation of extreme contact behaviors, such as those that would exploit point and edge contacts to maneuver within the environment. Here, our proposed methods provide the support for the manipulation of contact CoP's with precision. Also, it would be interesting to analyze contact singularities, such as the case due to stretching the knees during walking behaviors.

In summary, we have presented a framework for the analysis and control of internal forces and moments acting on closed loops formed by multicontact interactions on humanoids. We have created a new instance of the virtual-linkage model to characterize the relationship between internal forces and CoM maneuvers with respect to reaction forces on supporting surfaces. The grasp/contact matrix associated with the virtual-linkage model provides the support to plan CoM maneuvers and internal-force behavior that comply with rotational and frictional contact constraints. We have analyzed the dynamic representation of contact closed loops and derived a structure to control internal forces orthogonally to tasks and CoM behaviors. We have integrated this controller into our previous framework for prioritized multitasking. Finally, we have studied various simulations demonstrating the capabilities of our models and control methods in challenging multicontact examples.

Appendix A

Derivation of Constrained Dynamics

The robot's generalized coordinates, including its global position and orientation in space and the position of its articulated joints can be fully described by the set

$$\{x_b,\ q\} = \{x_{b,p},\ x_{b,r},\ q_1,\ q_2, \ldots,\ q_n\} \tag{63}$$

where the 6×1 vector $x_b = \{x_{b,p},\ x_{b,r}\}$ represents the position and orientation coordinates of a base reference located on the robot's body, and the $n \times 1$ vector q represents joint positions.

Reaction forces appear on supporting surfaces due to the effects of gravity forces and CoM accelerations. Using Lagrangian formalism and expressing the system's kinetic energy in terms of the joint kinetic and potential energies, we can derive the following equation of motion describing robot dynamics under supporting contacts:

$$A \begin{pmatrix} \dot{\vartheta}_b \\ \ddot{q} \end{pmatrix} + b + g + J_s^T F_r = \begin{pmatrix} 0 \\ \Gamma \end{pmatrix}. \tag{64}$$

Note that the actuation vector in the RHS of the above equation has six zeros corresponding to the six passive degrees of freedom (DOFs) associated with the robot's unactuated base. Moreover, the term $J_s^T F_r$ corresponds to the projection of reaction forces acting on contact extremities into forces acting on passive and actuated DOFs.

By left-multiplying the above equation by the term $J_s A^{-1}$ and considering the equality

$$\dot{\vartheta}_s = J_s \begin{pmatrix} \dot{\vartheta}_b \\ \ddot{q} \end{pmatrix} + \dot{J}_s \begin{pmatrix} \vartheta_b \\ \dot{q} \end{pmatrix} \tag{65}$$

we obtain the following equation of motion for the supporting extremities:

$$\dot{\vartheta}_s - \dot{J}_s \begin{pmatrix} \vartheta_b \\ \dot{q} \end{pmatrix} + J_s A^{-1}(b+g) + J_s A^{-1} J_s^T F_r = J_s A^{-1} U^T \Gamma. \quad (66)$$

Solving the above equation for the nonholonomic-contact constraints of (19), we obtain the estimate of reaction forces in terms of the actuation torques, which is given in (20). Substituting the above equation into (64), we obtain the constrained dynamic equation given in (25). QED

APPENDIX B

ANALYSIS OF CONTACT CENTERS-OF-PRESSURE AND CENTER-OF-MASS BEHAVIOR

We consider first the special case of bipedal coplanar multicontact stance. Since the dominant method for control of CoM maneuvers in biped stance is the ZMP, our initial premise is that ZMP trajectories are first provided. The question is what codependencies in the multicontact representation appear in such scenarios (see Fig. 9). We will see that the positions of the two contact CoP's depend on each other as a function of the ZMP. The ZMP is derived from the following equation of motion that balances moments on the robot [33]:

$$OP \times f_r + m_r = OG \times f_{\text{com}} + m_{\text{com}} \quad (67)$$

where P is a vector indicating ZMP coordinates, f_r is the vector of total resultant forces, m_r is the vector of total resultant moments about P expressed in global frame, and f_{com} and m_{com} are vectors of inertial and gravitational forces and moments measured at the robot's CoM. The solution of the above equation that renders zero resultant tangential moments about P correspond to the ZMP and can be found in [33]. Using P, we formulate the balance between moments about the ZMP with respect to moments about the two coplanar contact CoP's

$$OP \times f_r + m_r = \sum_{i=1}^{2} P_i \times f_{ri} + \sum_{i=1}^{2} m_{ri} \quad (68)$$

where f_{ri} and m_{ri} are the resultant reaction force and moment projected about the ith contact CoP. Solving the above equation for zero tangential moments (i.e., the ZMP condition $[m_r]^{\mathcal{T}} = 0$), we obtain the expression of the ZMP with respect to contact CoP's as

$$P_x = \sum_{i=1}^{2} \frac{P_{ix} f_{r_{iz}}}{f_{rz}} - \sum_{i=1}^{2} \frac{P_{iz} f_{r_{ix}}}{f_{r_z}} \overset{P_{iz}=0}{=} \sum_{i=1}^{2} \frac{P_{ix} f_{r_{iz}}}{f_{rz}} \quad (69)$$

$$P_y = \sum_{i=1}^{2} \frac{P_{iy} f_{r_{iz}}}{f_{rz}} - \sum_{i=1}^{2} \frac{P_{iz} f_{r_{iy}}}{f_{r_z}} \overset{P_{iz}=0}{=} \sum_{i=1}^{2} \frac{P_{iy} f_{r_{iz}}}{f_{rz}} \quad (70)$$

Here, we have used the coplanar condition $P_{1z} = P_{2z} = P_z = 0$, and the CoP condition $[m_{ri}]^{\mathcal{T}_i} = 0$. Using the equality $f_{rz} = \sum_{i=1}^{2} f_{r_{iz}}$, we define the fractional values as follows:

$$\alpha \triangleq \frac{f_{r1z}}{f_{rz}} \quad (71)$$

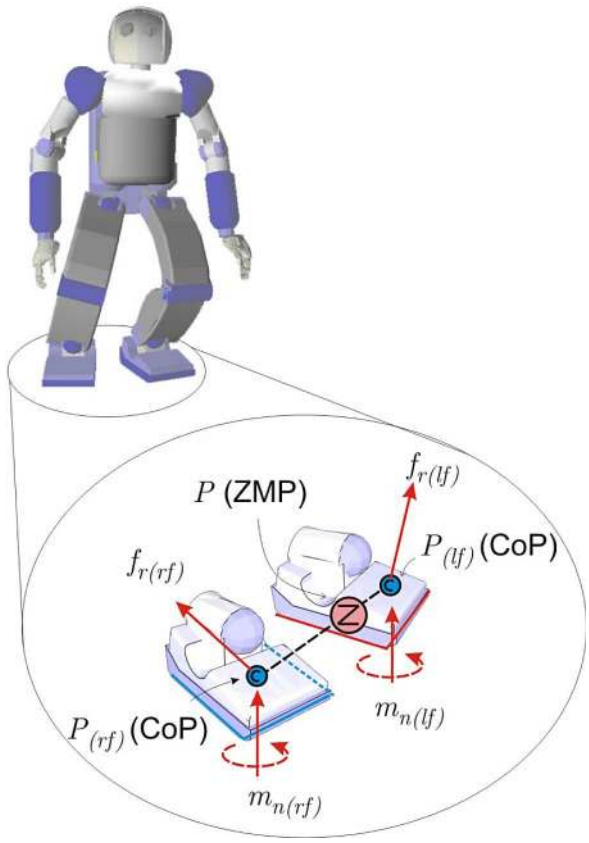

Fig. 9. Dependency between contact CoP's and ZMP. During biped coplanar contact stance, contact CoP's lie in a line that passes through the ZMP.

$$(1-\alpha) = \frac{f_{r2z}}{f_{rz}}. \quad (72)$$

Using (69), we formulate the equality $P_x = P_{1x}\alpha + P_{2x}(1-\alpha)$. Solving for α, we get

$$\alpha = \frac{P_{2x} - P_x}{P_{2x} - P_{1x}}. \quad (73)$$

Substituting α into (70) and solving for P_{2y}, we get

$$P_{2y} = P_y \frac{P_{2x} - P_{1x}}{P_x - P_{1x}} - P_{1y} \frac{P_{2x} - P_x}{P_x - P_{1x}}. \quad (74)$$

This relationship embodies two important characteristics. First, due to the dependency of P_{2y} on P, P_{1x}, P_{2x}, and P_{1y}, when P (i.e., the ZMP) is first determined, it is only possible to independently specify three coordinates from the four 2-D coordinates defining contact CoP positions. Second, the line uniting P_1 and P_2 passes through P. This can be seen by setting $P_{2y} = P_y$ and observing that $P_{2x} = P_x$. As a result, when we define a virtual-linkage model for biped coplanar behaviors, we can only consider controlling three of the four CoP quantities for a given ZMP trajectory.

When contacts are noncoplanar such as when they occur at different inclined surfaces, at surfaces with different heights, or when more than two contacts are involved in the stance, the dependencies implied by (74) do not apply. For example, consider the case of three coplanar contacts. Similar relationships as the

ones shown in (69) and (70) can be drawn by involving three summation terms on the RHS corresponding to the three contacts. Additionally, $f_r = f_{r1} + f_{r2} + f_{r3}$ involves three terms, and therefore, dependencies similar to (71) and (72) are now more complicated. Instead, we consider the ratios

$$\alpha \triangleq \frac{f_{r1z}}{f_{rz}}, \qquad \beta \triangleq \frac{f_{r2z}}{f_{rz}}, \qquad (1-\alpha-\beta) = \frac{f_{r3z}}{f_{rz}} \quad (75)$$

and then, using equations similar to (69) and (70), but involving three terms on the RHS, we can write

$$P_x = P_{1x}\alpha + P_{2x}\beta + P_{3x}(1-\alpha-\beta) \quad (76)$$

$$P_y = P_{1y}\alpha + P_{2y}\beta + P_{3y}(1-\alpha-\beta). \quad (77)$$

In the above equations, we observe that the contact CoP's P_1, P_2, and P_3 enclose P (i.e., the ZMP) within their triangular convex hull. This can be seen by plotting the solutions of P for the set $0 \leq \alpha \leq 1$ and $0 \leq \beta \leq 1-\alpha$. As a result, all the coordinates of the CoP points can be independently manipulated provided that they enclose the desired ZMP location.

It is also interesting to observe that the above equations reveal the usefulness of the ZMP in coplanar contact stance. Observing (69) and (70) for the bipedal case, we can see that when P approaches the location of a given P_i then the normal force of the opposing CoP becomes zero (i.e., if $P = P_1$, then $f_{r2z} = 0$, or if $P = P_2$, then $f_{r1z} = 0$). Therefore, P is confined within the line segment uniting the P_i's to avoid violation of unilateral contact constraints (i.e., $f_{riz} \geq 0$). In the case of coplanar tricontact stance, as defined in (76) and (77), a similar intuitive rule applies. When P approaches a given vertex in the convex hull (i.e., $P = P_i$), then the normal forces on the other two CoP's become zero. Moreover, when P approaches the line segments uniting two P_i's (i.e., the edges of the convex hull formed by the CoP's), then the normal force on the opposing CoP becomes zero (e.g., if $P = P_1\alpha + P_2(1-\alpha)$, then $f_{r3z} = 0$). These relationships are derived from basic exploration of the above equations. In summary, we have demonstrated that in coplanar contact cases, the ZMP must remain inside the convex hull of the CoP's to prevent violation of unilateral contact constraints.

We also consider the case where contacts are noncoplanar. First, we study noncoplanar biped stance, e.g., a human or humanoid robot standing with one foot on the floor and another foot against the wall, or with one foot on a stair and the other foot on the next one. The CoP's P_i now need to be specified as 3-D variables, since they lie on surfaces at different heights. The question is whether there exists similar interdependencies between CoP's as with the case of coplanar biped contact stance. The answer is no, they do not exist. For such cases, a ZMP, in a general sense, can be assigned (i.e., a point in space where the tangential moments about a desired surface vanish), but now, such point cannot be linked to unilateral contact conditions. Solving (68) now leads to the following equality:

$$P_x = \sum_{i=1}^{n_s} \frac{P_{ix} f_{r_{iz}}}{f_{rz}} - \sum_{i=1}^{n_s} \frac{P_{iz} f_{r_{ix}}}{f_{r_z}} - \sum_{i=1}^{n_s} \frac{{}^{y}R_i \, {}^{i}m_{riz}}{f_{rz}} \quad (78)$$

$$P_y = \sum_{i=1}^{n_s} \frac{P_{iy} f_{r_{iz}}}{f_{rz}} - \sum_{i=1}^{n_s} \frac{P_{iz} f_{r_{iy}}}{f_{r_z}} + \sum_{i=1}^{n_s} \frac{{}^{x}R_i \, {}^{i}m_{riz}}{f_{rz}} \quad (79)$$

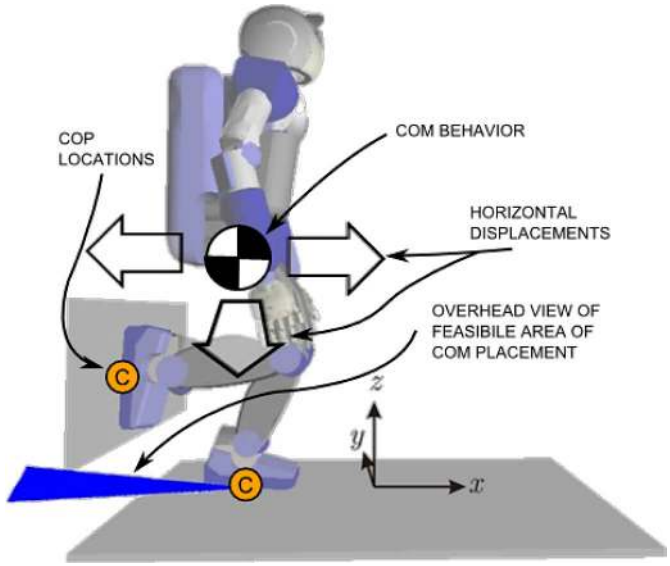

Fig. 10. Feasible area of CoM placement. This image illustrates the feasible area of CoM-static placement. The shaded triangular area shows the set of feasible locations of the horizontal components of the CoM. The vertical component of the CoM can be arbitrarily placed as we only need to consider gravitational forces for the static case.

where we observe that the terms P_{iz} now appear and that there are tangential moments in global frame induced by the normal moments on surfaces noncoplanar to the ZMP plane. Here, we have chosen a virtual horizontal frame to express the ZMP and used the condition $P_z = 0$. Also, the variables ${}^{i}m_{riz}$ represent the normal moments at the CoP points expressed in surface frames, and ${}^{x}R_i$ and ${}^{y}R_i$ are rotational matrices from local frames to the ZMP plane defined by the tangential coordinates x and y.

In the above case, if the ZMP approaches the contact CoP's, unilateral contact constraints are not necessarily violated. Let us consider a biped noncoplanar stance with $P = P_1$. This case does not imply that f_{r2z} is equal to zero as it was in the coplanar case, since (78) and (79) have now moment components that allow excursions of the ZMP beyond the convex hull.

Let us explore this case in more detail through the scenario depicted in Fig. 10, which involves one foot placed on the wall. We first analyze the static case where the robot's CoM does not move. The question is what is the set of feasible CoM locations. In static stance, the ZMP becomes equal to the ground projection of the CoM. This can be seen by solving (67), which leads to the following equalities:

$$P_x = G_x - \frac{G_z f_{rx}}{f_{rz}} - \frac{m_{\mathrm{com}_y}}{f_{rz}} \quad (80)$$

$$P_y = G_y - \frac{G_z f_{ry}}{f_{rz}} + \frac{m_{\mathrm{com}_x}}{f_{rz}}. \quad (81)$$

When the robot is not moving, $f_{rx} = f_{ry} = 0$, and $m_{\mathrm{com}} = 0$. As a result $P_x = G_x$, and $P_y = G_y$.

Similarly to the analysis of the feasible CoM locations discussed in Section IV, we use (47) to plot the stability area under frictional constraints. We observe that this is not a line as it

would be in coplanar bipedal stance. Instead, it is a triangular region reaching behind the foot on the wall and to the sides of the sagittal plane. Exploring (78) and (79), we observe that the reason why the CoM can be placed behind the wall is because there exists normal forces against the wall in the x-direction. On the other hand, the offsets of the CoM in the y-direction are counteracted by reaction forces in the y-direction (i.e., the forces tangential to the wall) or by contact reaction moments in the x-direction (i.e., moments normal to the wall).

To analyze dynamic CoM maneuvers during complex multicontact situations, the above equations involving the ZMP become more difficult to use. For this reason, the model of (47) derived from the virtual-linkage model appears as a strong candidate to study and develop dynamic and static maneuvers in all contact situations. This model can be queried for desired CoM maneuvers, and in combination with an optimal solver, it can be used to estimate internal-force trajectories that comply with frictional properties. This technique is now the next focus of our research.

APPENDIX C

SPECIAL VIRTUAL-LINKAGE MODELS FOR BIPEDAL STANCES

Let us focus on the coplanar bipedal CoP dependencies, as given in (68)–(74). Similarly to the dependencies associated with dual contact behaviors described in the original virtual-linkage model [35], the dependency between ZMP and contact CoP's for two-contact stance, as described previously, restricts the number of contact moments that can be controlled. Only five contact moments can be controlled instead of the six that would be expected. To solve this problem, we associate a special case of virtual-linkage model with three contact CoP coordinates instead of four. If the set of internal moments were to contain four tangential CoP coordinates and the normal moments, the virtual-linkage model of (13) would be overdetermined and, therefore, not fully controllable.

To understand this reduction, we observe that during two-contact interactions, there exist six internal forces between the contacts and six resultant forces associated with the robot's CoM behavior. Equation (13) defines the relationship between CoM and internal forces and moments with respect to reaction forces. The six CoM forces and moments determine the ZMP's behavior and, therefore, impose the dependencies with respect to the CoP's, thus limiting the number of internal moments that can be controlled. Therefore, we define a different virtual-linkage model for bipedal coplanar contacts involving the tension between the two contacts, the two normal moments of the contacts, and only three out of four tangential moments (see Fig. 11). The reduced set of internal forces and moments describing the virtual-linkage model for bipedal contact is, therefore, equal to

$$F_{\text{int}} = \begin{pmatrix} f_{\text{int}} \\ \hline m_{\text{int}} \end{pmatrix} \triangleq \begin{pmatrix} f_t \\ \hline m_{\text{cop}(rf)(2d)} \\ m_{\text{cop}(lf)(1d)} \\ m_{n(rf)} \\ m_{n(lf)} \end{pmatrix} \epsilon \mathcal{R}^6. \qquad (82)$$

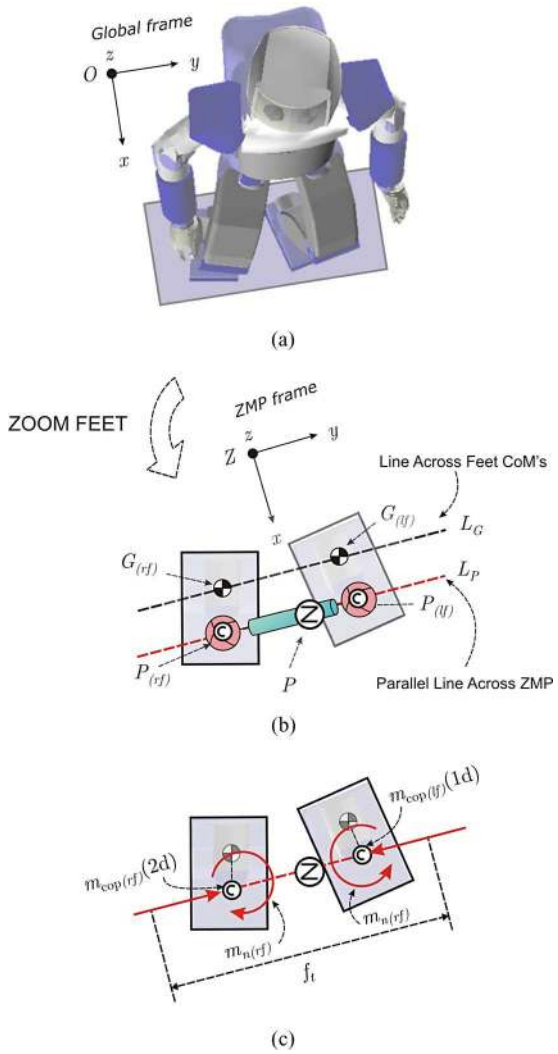

Fig. 11. Virtual-linkage model in bipedal stance. (a) Top view of the robot. (b) Virtual-linkage model involving two spherical joints and one prismatic joint. The point P is the ZMP and the points C are the contact CoP's. As discussed earlier, the ZMP lies on the line connecting the two CoP's. The black and white circles correspond to the CoMs of the feet links. To simplify the control of CoP's, we choose them to lie in a line parallel to the segment connecting the feet CoM's. (c) Six internal forces and moments that are independently controllable given ZMP trajectories. This corresponds to one tension force, two normal moments, and three out of four coordinates of the CoP's.

The behavior of the CoM with respect to contact reaction forces, as described in (12), remains the same.

The case of noncoplanar bipedal contact stance needs also a special virtual-linkage model, since there exist also six independent internal-force and moment quantities. However, in noncoplanar bipedal contact stance, the four coordinates describing the two CoP's can now lie outside of the line connecting the ZMP (as analyzed in Fig. 10). Therefore, two more internal quantities besides the contact CoP's can be independently controlled. Our choice is to control the two normal moments about the contact surfaces and ignore the tension force. Another valid choice would be to control the tension force and one out of the two normal moments. Our choice leads to the following specification of the virtual-linkage model for noncoplanar bipedal

contact stance

$$F_{\text{int}} = m_{\text{int}} \triangleq \begin{pmatrix} m_{\text{cop}(rf)(2d)} \\ m_{\text{cop}(lf)(2d)} \\ m_{n(rf)} \\ m_{n(lf)} \end{pmatrix} \epsilon\, \mathcal{R}^6. \tag{83}$$

Once more, the behavior of the CoM with respect to contact reaction forces described in (12) remains the same.

APPENDIX D

MATRICES FOR THE VIRTUAL-LINKAGE MODEL

In this section, we specify the algebraic expressions of the matrices used in (8), (10), and (11) that define the internal forces and moments of the virtual-linkage model.

First, we specify the matrices involved in the expression of CoP moments. The matrix T_s represents the cumulative spatial transformation matrix from global frame to surface frames. For the sake of simplicity, it is convenient to express this matrix with respect to a rearranged version of the vector of reaction forces of (20), where forces and moments appear in pairs, i.e.,

$$F_{r,fm} \triangleq \begin{pmatrix} f_{r1} \\ \hline m_{r1} \\ \vdots \\ \hline f_{rn_s} \\ m_{rn_s} \end{pmatrix} = S_{fm} \begin{pmatrix} f_{r1} \\ \vdots \\ f_{rn_s} \\ \hline m_{r1} \\ \vdots \\ m_{rn_s} \end{pmatrix} = S_{fm} F_r \tag{84}$$

where S_{fm} is a selection matrix rearranging the order of the reaction forces. Given the above rearrangement, the vector of reaction forces on the RHS of (8) can be first premultiplied by S_{fm}, and then, the cumulative spatial transformation can be applied, i.e.,

$$T_s \triangleq \begin{pmatrix} T_{P1} & [0]_{3\times 6} & [0]_{3\times 6} & \cdots \\ [0]_{3\times 6} & T_{P_2} & [0]_{3\times 6} & \vdots \\ & & \ddots & \\ [0]_{3\times 6} & \cdots & [0]_{3\times 6} & T_{P_{n_s}} \end{pmatrix} \cdot S_{fm} \epsilon\, \mathcal{R}^{6n_s \times 6n_s} \tag{85}$$

where each component is the standard spatial transformation for pairs of forces and moments defined by

$$T_{P_i} \triangleq ((G_i - P_i) \times R_{P_i} | R_{P_i}) \epsilon\, \mathcal{R}^{3\times 6} \tag{86}$$

where G_i is the position of the CoM of the ith supporting link, P_i is its CoP point, and R_{P_i} is the rotation matrix from global frame to the frame oriented with respect to the surface below the contact link. After applying the above spatial transformations, we select the tangential moments with respect to surface tangential coordinates using the matrix

$$S_{\text{cop}} \triangleq \left(\begin{array}{c|c|c} \begin{matrix} 000100 \\ 000010 \end{matrix} & [0]_{2\times 6} & \cdots \\ \hline [0]_{2\times 6} & \ddots & \vdots \\ \hline \vdots & \cdots & \begin{matrix} 000100 \\ 000010 \end{matrix} \end{array}\right) \epsilon\, \mathcal{R}^{2n_s \times 6n_s}. \tag{87}$$

Next, we specify the matrices involved in the representation of the $3(n_s - 2)$ vector of tension forces. Based on (10), we first take the $9(n_s - 2)$ differences between pairs of linear forces. The following matrix shows an instance of a differential matrix for the virtual-linkage model of Fig. 4, where there exists four contact links and six tension forces:

$$\Delta_t \triangleq \left(\begin{array}{cccc|cccc} I & -I & 0 & 0 & 0 & 0 & 0 & 0 \\ I & 0 & -I & 0 & 0 & 0 & 0 & 0 \\ I & 0 & 0 & -I & 0 & 0 & 0 & 0 \\ 0 & I & -I & 0 & 0 & 0 & 0 & 0 \\ 0 & I & 0 & -I & 0 & 0 & 0 & 0 \\ 0 & 0 & I & -I & 0 & 0 & 0 & 0 \end{array}\right) \epsilon\, \mathcal{R}^{9(n_s-2)\times 6n_s} \tag{88}$$

where I is the identity matrix; in this case, it is of dimension 3×3. The first row corresponds to the differential of forces between the right hand and the left hand, the second row corresponds to the differential between the right hand and the right foot, the third row corresponds to the differential between the right hand and the left foot, etc., until we express the six tension differentials.

The rotation matrix R_t takes differential forces expressed in global frame and rotates them along the links of the virtual-linkage model using the following expression for the case of Fig. 4:

$$R_t = \begin{pmatrix} R_{12} & 0 & 0 & 0 & 0 & 0 \\ 0 & R_{13} & 0 & 0 & 0 & 0 \\ 0 & 0 & R_{14} & 0 & 0 & 0 \\ 0 & 0 & 0 & R_{23} & 0 & 0 \\ 0 & 0 & 0 & 0 & R_{24} & 0 \\ 0 & 0 & 0 & 0 & 0 & R_{34} \end{pmatrix} \epsilon\, \mathcal{R}^{9(n_s-2)\times 9(n_s-2)} \tag{89}$$

$$R_{ij} = \begin{pmatrix} \widehat{x}_{ij}^T \\ \widehat{y}_{ij}^T \\ \widehat{z}_{ij}^T \end{pmatrix}$$

$$\begin{cases} \widehat{x}_{ij} = \frac{P_i - P_j}{\|P_i - P_j\|} \\ \widehat{y}_{ij} = (\, -\hat{x}_{ij}(2) \quad \hat{x}_{ij}(1) \quad 0\,)^T \\ \widehat{z}_{ij} = \widehat{x}_{ij} \times \widehat{y}_{ij}. \end{cases} \tag{90}$$

which result on the x-component aligned with the links. To obtain the tension forces, all is needed is to select the x-directions using the selection matrix

$$S_t \triangleq \begin{pmatrix} 1 & 0 & 0 & [0]_{1\times 3} & [0]_{1\times 3} & \cdots \\ [0]_{1\times 3} & 1 & 0 & 0 & [0]_{1\times 3} & \vdots \\ & & & & \ddots & \\ [0]_{1\times 3} & & \cdots & & [0]_{1\times 3} & 1 \quad 0 \quad 0 \end{pmatrix} \epsilon \mathcal{R}^{3(n_s-2)\times 9(n_s-2)}. \quad (91)$$

Finally, we specify the matrices involved in the expression of normal moments of (11). We note that it involves a spatial transformation from global frame to surface local frames using the previous definition of T_s. However, this time we choose the normal-moment components using the following selection matrix also specify for the particular case of Fig. 4:

$$S_n \triangleq \begin{pmatrix} 0\cdots 01 & [0]_{1\times 6} & [0]_{1\times 6} & [0]_{1\times 6} \\ [0]_{1\times 6} & 0\cdots 01 & [0]_{1\times 6} & [0]_{1\times 6} \\ [0]_{1\times 6} & [0]_{1\times 6} & 0\cdots 01 & [0]_{1\times 6} \\ [0]_{1\times 6} & [0]_{1\times 6} & [0]_{1\times 6} & 0\cdots 01 \end{pmatrix} \epsilon \mathcal{R}^{n_s\times 6n_s}. \quad (92)$$

ACKNOWLEDGMENT

The authors would like to thank T. Yoshikawa for his contributions and R. Philippsen and P. Fraisse for reviewing this paper.

REFERENCES

[1] C. O. Alford and S. M. Belyeu, "Coordinated control of two robot arms," in *Proc. IEEE Int. Conf. Robot. Autom.*, Mar. 1984, pp. 468–473.
[2] T. Bretl and S. Lall, "Testing static equilibrium for legged robots," *IEEE Trans. Robot.*, vol. 24, no. 4, pp. 794–807, Aug. 2008.
[3] J. Buchli, F. Iida, and A. J. Ijspeert, "Finding resonance: Adaptive frequency oscillators for dynamic legged locomotion," in *Proc. IEEE/RSJ Int. Conf. Intell. Robots Syst.*, 2006, pp. 3903–3909.
[4] K. C. Chang and O. Khatib, "Operational space dynamics: Efficient algorithms for modeling and control of branching mechanisms," in *Proc. IEEE Int. Conf. Robot. Autom.*, Apr. 2000, pp. 850–856.
[5] C. Collette, A. Micaelli, C. Andriot, and P. Lemerle, "Robust balance optimization control of humanoid robots with multiple non coplanar grasps and frictional contacts," in *Proc. IEEE Int. Conf. Robot. Autom.*, Pasadena, CA, May 2008, pp. 3187–3193.
[6] S. Collins, A. Ruina, R. Tedrake, and M. Wisse, "Efficient bipedal robots based on passive-dynamic walkers," *Sci. Mag.*, vol. 307, no. 5712, pp. 1082–1085, 2005.
[7] E. Demircan, L. Sentis, V. DeSapio, and O. Khatib, "Human motion reconstruction by direct control of marker trajectories," presented at the 11th Int. Symp. Adv. Robot Kinematics, Batz-sur-Mer, France, Jun. 2008.
[8] A. A. Frank, "Control systems for legged locmotion machines," Ph.D. dissertation, Univ. Southern California, Los Angeles, CA, 1968.
[9] D. T. Greewood, *Principles of Dynamics*. Englewood Cliffs, NJ: Prentice-Hall, 1988.
[10] K. Harada, S. Kajita, K. Kaneko, and H. Hirukawa, "Zmp analysis for arm/leg coordination," in *Proc. IEEE/RSJ Int. Conf. Intell. Robots Syst.*, Las Vegas, NV, Oct. 2003, pp. 75–81.
[11] K. Hirai, M. Hirose, Y. Haikawa, and T. Takenaka, "The development of Honda humanoid robot," in *Proc. IEEE Int. Conf. Robot. Autom.*, Leuven, Belgium, vol. 2, pp. 1321–1326, 1998.
[12] R. Holmberg and O. Khatib, "Development and control of a holonomic mobile robot for mobile manipulation tasks," *Int. J. Robot. Res.*, vol. 19, no. 11, pp. 1066–1074, 2000.
[13] S.-H. Hyon, J. Hale, and G. Cheng, "Full-body compliant human humanoid interaction: Balancing in the presence of unknown external forces," *IEEE Trans. Robot.*, vol. 23, no. 5, pp. 884–898, Oct. 2007.
[14] A. J. Ijspeert, J. Buchli, A. Selverston, M. Rabinovich, M. Hasler, W. Gerstner, A. Billard, H. Markram, and D. Floreano, Eds., "Dynamical principles for neuroscience and intelligent biomimetic devices," presented at the EPFL-LATSIS Symp., Lausanne, Switzerland, 2006.
[15] O. Khatib, "Commande dynamique dans l'espace opérationnel des robots manipulateurs en présence d'obstacles," Ph.D. dissertation, l'École Nationale Supérieure de l'Aéronautique et de l'Espace, Toulouse, France, 1980.
[16] O. Khatib, "A unified approach for motion and force control of robot manipulators: The operational space formulation," *Int. J. Robot. Res.*, vol. 3, no. 1, pp. 43–53, 1987.
[17] O. Khatib, "Object manipulation in a multi-effector robot system," in *Robotics Research 4*, R. Bolles and B. Roth, Eds. Cambridge, MA: MIT Press, 1988, pp. 137–144.
[18] O. Khatib, L. Sentis, and J. Park, "A unified framework for whole-body humanoid robot control with multiple constraints and contacts," in *Springer Tracts in Advanced Robotics—STAR Series*. Prague, Czech Republic, Mar. 2008.
[19] O. Khatib, P. Thaulaud, and J. Park, "Torque-position transformer for task control of position controlled robots," Patent 20 060 250 101, Nov. 2006.
[20] T. McGeer, "Passive dynamic walking," *Int. J. Robot. Res.*, vol. 9, no. 2, pp. 62–68, 1990.
[21] Y. Nakamura, H. Hanafusa, and T. Yoshikawa, "Mechanics of coordinative manipulation by multiple robotic mechanisms," in *Proc. IEEE Int. Conf. Robot. Autom.*, Apr. 1987, pp. 991–998.
[22] J. Park, "*Control Strategies For Robots In Contact*," Ph.D. dissertation, Stanford Univ., Stanford, CA, 2006.
[23] R. Philippsen, N. Negati, and L. Sentis, "Bridging the gap between semantic planning and continuous control for mobile manipulation using a graph-based world representation," presented at the Workshop Hybrid Control Auton. Syst., Pasadena, CA, Jul. 2009.
[24] M. H. Raibert, M. Chepponis, and H. B. Brown, "Running on four legs as though they were one," *IEEE J. Robot. Autom.*, vol. RA-2, no. 2, pp. 70–82, Jun. 1986.
[25] M. H. Raibert and J. J. Craig, "Hybrid position force control of manipulators," *ASME J. Dyn. Syst. Meas. Control*, vol. 103, no. 2, pp. 126–133, 1981.
[26] D. Ruspini and O. Khatib, "Collision/contact models for dynamic simulation and haptic interaction," in *Proc. 9th Int. Symp. Robot. Res.*, Snowbird, UT, Oct. 1999, pp. 185–195.
[27] L. Sentis, "Synthesis and control of whole-body behaviors in humanoid systems," Ph.D. dissertation, Stanford Univ., Stanford, CA, 2007.
[28] L. Sentis and O. Khatib, "Task-oriented control of humanoid robots through prioritization," in *Proc. IEEE/RSJ Int. Conf. Humanoid Robots*, Los Angeles, CA, Nov. 2004, pp. 475–480.
[29] L. Sentis and O. Khatib, "Synthesis of whole-body behaviors through hierarchical control of behavioral primitives," *Int. J. Humanoid Robot.*, vol. 2, no. 4, pp. 505–518, Dec. 2005.
[30] A. Takanishi, M. Ishida, Y. Yamazaki, and I. Kato, "The realization of dynamic walking robot wl-10rd," in *Proc. Int. Conf. Adv. Robot.*, 1985, pp. 459–466.
[31] A. Takanishi, H. O. Lim, M. Tsuda, and I. Kato, "Realization of dynamic biped walking stabilized by trunk motion on sagitally uneven surface," in *Proc. IEEE/RSJ Int. Conf. Intell. Robots Syst.*, 1990, pp. 323–330.
[32] R. Tedrake, T.W. Zhang, M. Fong, and H.S. Seung, "Actuating a simple 3d passive dynamic walker," in *Proc. IEEE Int. Conf. Robot Autom.*, 2004, pp. 4656–4661.
[33] M. Vukobratović and B. Borovac, "Zero-moment point thirty five years of its life," *Int. J. Humanoid Robot.*, vol. 1, no. 1, pp. 157–173, 2004.
[34] E. R. Westervelt, J. W. Grizzle, C. Chevallereau, J. H. Choi, and B. Morris, *Feebdack Control of Dynamic Bipedal Robot Locomotion*. Boca Raton, FL: CRC, 2007.
[35] D. Williams and O. Khatib, "The virtual linkage: A model for internal forces in multi-grasp manipulation," in *Proc. IEEE Int. Conf. Robot. Autom.*, Atlanta, GA, Oct. 1993, pp. 1025–1030.

Luis Sentis (M'09) received the B.S. degree from the Polytechnic University of Catalonia, Barcelona, Spain, in 1996 and the Ph.D. degree from Stanford University, Stanford, CA, in 2007.

He is currently an Assistant Professor with the Department of Mechanical Engineering at the University of Texas at Austin, where he is engaged in biomechatronics design, models and controllers for compliant grasping, and virtual reality environments. Between 1996 and 1998, he was a Control and Research Engineer in Silicon Valley. His current research interests include modeling multicontact compliant behaviors for whole-body manipulation and locomotion. He is a Codesigner of the Whole-Body Control Framework, which is an open-source embedded controller built for Willow Garage, Inc.'s, Robot Operating System.

Jaeheung Park (M'10) received the B.S. and M.S. degrees in aerospace engineering from Seoul National University, Seoul, Korea, in 1995 and 1999, respectively, and the Ph.D. degree in aeronautics and astronautics from Stanford University, Stanford, CA, in 2006.

From 2006 to 2009, he was a Postdoctoral Researcher and, later, a Research Associate at the Stanford Artificial Intelligence Laboratory. From 2007 to 2008, he was with Hansen Medical, Inc. (part time), which is a medical robotics company in the U.S. Since 2009, he has been an Assistant Professor with the Department of Intelligent Convergence Systems, Seoul National University. His current research interests include robot–environment interaction, contact-force control, robust haptic teleoperation, multicontact control, whole-body dynamic control, biomechanics, and medical robotics.

Oussama Khatib (M'85–SM'98–F'03) received the Ph.D. degree from Sup'Aero, Toulouse, France, in 1980.

He is currently a Professor of computer science with Stanford University, Stanford, CA. He is a Coeditor of *The Robotics Review* (MIT Press), the *Springer Tracts in Advanced Robotics*, and the *Springer Handbook of Robotics*. His research interests include human-centered robotics, haptic interactions, and human-friendly robot design.

Prof. Khatib was the Program Chair of the 2000 IEEE International Conference on Robotics and Automation, San Francisco, CA. He is the President of the International Foundation of Robotics Research. He was a Distinguished Lecturer of the IEEE and is a recipient of the Japan Robot Association (JARA) Award.